Received: 16 July 2019 | Revised: 8 October 2019 | Accepted: 5 November 2019 | Published on: 25 December 2019

DOI: 10.1002/qj.3711

Quarterly Journal of the Royal Meteorological Society RMetS

RESEARCH ARTICLE

Sensitivity study of the planetary boundary layer and microphysical schemes to the initialization of convection over the Arabian Peninsula

Thomas Schwitalla | Oliver Branch | Volker Wulfmeyer

Institute of Physics and Meteorology, University of Hohenheim, Stuttgart, Germany

Correspondence
T. Schwitalla, Institute of Physics and Meteorology, University of Hohenheim, Garbenstrasse 30, 70599 Stuttgart, Germany.
Email: thomas.schwitalla@uni-hohenheim.de

Funding information
UAE Research Program for Rain Enhancement Science (UAEREP)

Abstract

In this study, we present a five-member Weather Research and Forecasting (WRF) physics ensemble over the Arabian Peninsula on the convection-permitting (CP) scale and investigate the ability to simulate convection and precipitation by varying the applied cloud microphysics and planetary boundary layer (PBL) parametrizations. The study covers a typical precipitation event ocurring during summertime over the eastern part of the United Arab Emirates (UAE). Our results show that the best results are obtained by using water- and ice-friendly aerosols combined with aerosol-aware Thompson cloud microphysics and the Mellor-Yamada-Nakanishi-Niino (MYNN) PBL parametrization. The diurnal cycle of 2-m temperature over the desert is well captured by all members, although a cold bias is present during the morning and evening transition. All members are capable of simulating the correct timing of the onset of convection. Simulations with the MYNN PBL and Thompson scheme produce the highest convective available potential energy (CAPE) and convective inhibition (CIN), associated with stronger mixing inside the PBL, leading to the formation of more dense liquid water clouds. The WDM6 microphysics scheme is not a suitable option, as there are hardly any liquid water clouds; mainly ice clouds are simulated. Precipitation is best captured by applying the MYNN and Thompson scheme. Although the ensemble size is relatively small, this allows for the provision of cloud probability maps suitable for cloud-seeding applications.

KEYWORDS
convection, ensemble, PBL, UAE, WRF

1 | INTRODUCTION

The climate of the Arabian peninsula is characterized by high temperatures and low precipitation amounts. However, annual cycles are still pronounced, with maxima of precipitation and minima of temperatures in winter. The meteorological situations in winter and the transition periods are driven by troughs moving southeastwards along Saudi Arabia, leading to prevalent northwesterly winds (Patlakas *et al.* 2019).

All authors contributed equally to this work.

Over the United Arab Emirates (UAE), these conditions result in annual precipitation amounts between 20 and 130 mm from west to east, which are produced mainly during the winter–springtime period, whereas the summertime precipitation is only around 20% of the annual precipitation.

The opposite is the case in summer. During summer, strong suppression of vertical motion is present, due to the subtropical high leading to a strong reduction of precipitation. However, upper-level disturbances from tropical monsoon flows are the main factor responsible for moisture transport toward the Arabian Peninsula (Böer, 1997; Al Mandoos, 2005).

Regardless of the small rain amounts in summer, favorable conditions for rain events can still exist, leading to convection initation (CI) over the Al Hajar mountain range and convergence zones over the west. The understanding and correct simulation of these effects is crucial for the prediction of extreme events and for the application of weather modification efforts like cloud seeding and and rain enhancement by using desert plantations (Branch and Wulfmeyer, 2019).

Favorable conditions are due to the low-level forcing of vertical motion in a rather diffuse section of the intertropical convergence zone (ITCZ) and due to land-surface heterogeneity. The latter is caused by sea-breeze effects and the orography in the Hajar mountains in the northeastern part of the country eventually leading to the development of convergence zones along the coast and over the Hajar mountain range. Therefore, though summertime is the driest period for the Arabian peninsula, a significant west–east gradient exists, with basically no rainfall over the deserts in the western and central part of the UAE, with amounts < 5 mm, but with increasing amounts up to ≈ 20 mm toward and over the Hajar mountain range (Wehbe *et al.* 2017; Mahmoud *et al.* 2019). The latter is produced by a series of CI events over the Al Hajar Mountains, which can propagate to the west depending on the local and large-scale forcing conditions (Böer, 1997; Sherif *et al.* 2014; Steinhoff *et al.* 2018; Wehbe *et al.* 2019).

Overall, these rain amounts correspond to a volume of 50 million m^3 of water during summer, which is by far insufficient to provide enough water for agriculture and daily life. The UAE requires around 1.74 billion m^3 of water[1] per year, which will increase further due to the rapid development of the population. Furthermore, the Arabian Sea is characterized by a high salinity of around 4%, so that the sea water cannot be used for irrigation and drinking water. Thus, seawater desalination is applied, which provides by far the majority of the required water, but this technique is very expensive and not sustainable.

Due to the lack of natural rain events and the complexity and expenses of the desalination efforts, the UAE started the investigation of cloud seeding for rain enhancement as early as the 1990s. Mainly, hygroscopic seeding was investigated and analyzed by statistical evaluation of the results. Bruintjes (1999), NCAR (2005), and Breed *et al.* (2007) showed that a positive impact of hygroscopic cloud seeding was not detectable within the error limits.

In order to get further insight into the understanding of the modification of clouds and rain amounts, the UAE Research Program for Rain Enhancement Science (UAEREP[2]) was launched by the UAE Ministry of Presidential Affairs in 2015. The major goals of the UAEREP are to advance the science of rain enhancement and to increase rainfall for water security in the UAE and other arid and semi-arid regions. One of the specialties of the UAEREP is that not only cloud seeding approaches are considered; rather, the research is rather general. Also, various other techniques and approaches are considered, such as changes of land-surface conditions and a variety of technical solutions. Currently, nine projects are funded in three funding cycles.

One of the projects in the first cycle was awarded to the University of Hohenheim (UHOH) in Stuttgart, Germany. This project is called Optimizing Cloud Seeding by Advanced Remote Sensing and Land Cover Modification (OCAL[3]). It is the first and only project in the UAEREP to study the potential of land-surface modifications to enhance rainfall in desert regions. OCAL has two main goals.

1. Provide the UAE with unique modeling and observational capabilities for improving cloud process understanding, forecasting, and cloud-seeding guidance.
2. Study the effect of land-surface modifications on the initiation and amplification of precipitation over the UAE.

This work focuses on the first item and reports its first results. This research activity is based on the following considerations.

- It is not sufficient to investigate the impact of cloud-seeding efforts merely by statistical analysis of experiments. Due to the absence of identical twin experiments and the complex cloud and precipitation development and evolution, statistical analyses will remain highly uncertain and often are not reliable.

[1]https://government.ae/en/information-and-services/environment-and-energy/water-and-energy/water-

[2]http://www.uaerep.ae/

[3] https://ocal.uni-hohenheim.de/en

- Therefore, advanced model systems must be developed and applied that are capable of simulating the preconvective environment, as well as the evolution of clouds and precipitation, with high temporal and spatial resolution and high predictive skill.
- The forecast accuracy needs to be be characterized by uncertainty estimates derived from ensemble simulations.

These are essential steps to advance rain enhancement research, because then the results can be used for cloud-seeding guidance, the simulation of other rain enhancement efforts, and the evaluation of the impact of cloud-seeding efforts without conducting long-term statistical experiments.

However, this requires excellent performance of the model system. The question arises: how should an ensemble forecast system be designed in order to reach these ambitious goals? Current understanding of research activities in ensemble-based weather forecasting reveal that it should be focused on the following issues.

1. The ensemble members must be operated on the convection-permitting (CP) scale (≈ 2 km), if not on the turbulence-permitting scale (100 m), in order to avoid parametrizations of deep convection and resolve land-surface heterogeneities and convergence zones (Bauer *et al.* 2011; Palmer, 2013; Schwitalla *et al.* 2017).
2. As computing power is a limiting factor for the operation of CP ensembles, a limited-area model (LAM) needs to be operated, which requires the forcing of the model system with global analyses. Therefore, the quality of these global analyses should be as accurate as possible.
3. The ensemble represents the model uncertainty with respect to initial conditions and model physics, so that it approaches as best as possible the limits of predictability (e.g., Evans *et al.* 2012; Palmer and Zanna, 2013; Zhu and Xue, 2016).
4. A data assimilation system needs to be applied to optimize the initial state of the model system.

In this work, we demonstrate the first results toward the design and operation of an ensemble forecasting system for the UAE. To our knowledge, this is the first effort to perform forecasts with uncertainty estimates over the Arabian Peninsula covering points 1–3 of the issues above. Data assimilation efforts using an advanced variational data assimilation system will be the subject of a future publication. Here, we present the setup and performance of a new five-member forecast ensemble with CP resolution, which was developed for quasi-operational forecasts over the UAE. We evaluate its performance for a complex CI case, where precipitation developed over the Al Hajar mountains with respect to various crucial variables, starting with surface fluxes, to surface atmospheric variables, to cloud and precipitation fields. According to a study of Niranjan Kumar and Ouarda (2014), the monthly mean rainfall amount for July near the mountains is about 0.2 mm. This very low amount of rainfall mean that a meaningful statistical evaluation is not feasible. There are simply not enough days during summer that have intense cloud development and a considerable amount of rainfall.

The article is laid out as follows. Section 2 provides the state-of-the-art of our understanding of the process chain leading to summertime CI, as well as the development of clouds and precipitation over the UAE. Section 3 describes the design of the ensemble. Section 4 gives an overview of the data sets applied for model verification. The meteorological conditions of the case are presented in section 5. Section 6 shows the results and analyzes the accuracy and the uncertainty of the results. The last section summarizes our results and gives an overview of necessary future activities to refine the results further.

2 | SUMMERTIME CONVECTION INITIATION OVER THE ARABIAN PENINSULA

The summer climate over the Arabian Peninsula is characterized by a heat low centered over Saudi Arabia with a central pressure of approx. 1000 hPa. This is a typical value over warm-season desert regions (Ackerman and Cox, 1982; Warner, 2004; Steinhoff *et al.* 2018). Due to the surface heating, the minimum pressure varies greatly during the daytime, leading to an even larger pressure gradient and thus higher wind speeds, potentially increasing surface convergence (Mohalfi *et al.* 1998).

During summertime, due to the large contrasts between sea-surface temperatures of the Arabian Gulf and the Gulf of Oman and air temperatures over land, a strong sea breeze develops during the daytime (Rácz and Smith, 1999), with an inland extent of more than 50 km (Eager *et al.* 2008). During the night, a land breeze exists along the coast, in combination with a low-level jet (Ranjha *et al.* 2015). The properties of this nocturnal jet determine the strength of the sea breeze on the following day. Due to high sensible heat fluxes over land and low-level wind shear induced by the sea breeze, boundary-layer convection is often organized by horizontal convective rolls (Weckwerth *et al.* 1997) while its structure is mainly determined by the ratio of the boundary-layer height z_i and the Monin–Obukhov length L (Weckwerth *et al.* 1999). Both the sea breeze and the convective rolls interact in such a way that the sea breeze provides moisture from the sea

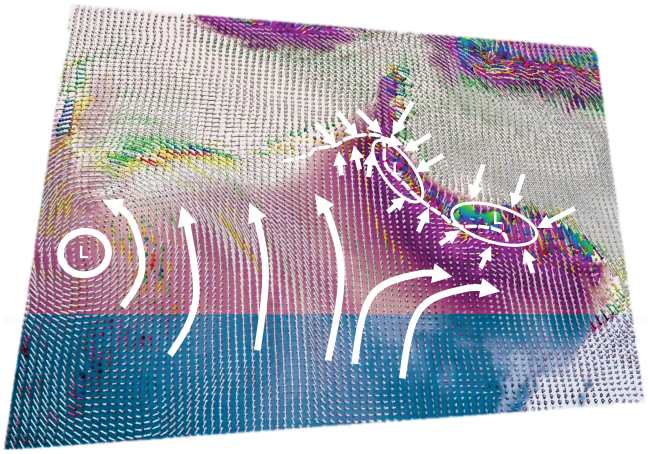

FIGURE 1 Schematic of the environmental conditions for convection initation. The Arabian heat low is located over Saudi Arabia, as seen in the left of the figure. During daytime, a strong sea breeze develops over the UAE and Oman. Together with the differential heating over the Al Hajar mountains, a heat low is induced, leading to convection initation along the white dashed line. Colored isosurfaces over the mountains indicate clouds, while the wind barbs show near-surface wind colored by vertical velocity

and the convective rolls transport the moisture further upwards.

Figure 1 shows a schematic of the relevant processes. Due to the steep mountain slopes in the Al Hajar Mountain range, differential surface heating plays an important role in the initiation of convection (Kottmeier *et al.* 2008). During daytime, the mountain slopes are heated by the sun and the air close to the ground is warming more rapidly than the adjacent air in the valleys. As the air density decreases with higher temperature, an upward motion starts to develop toward the mountain slope, resulting in the development of a localized low-pressure system.

The convergence over the mountains is enhanced by the northwesterly flow from the Arabian Gulf and the easterly flow from the Gulf of Oman toward the Al Hajar mountains associated with the land–sea breeze occurring during daytime.

To support this theory, Figure 2 shows the 10-m wind speed and direction from the European Centre for Medium-Range Weather Forecasts (ECMWF) operational analysis averaged for June, July, and August 2015 at 1200 UTC (4:00 pm local time). Although some daytime convergence zones can be detected in the western part of the UAE, near the border toward Saudi Arabia (Steinhoff *et al.* 2018), the strongest convergence occurs over the Al Hajar mountains.

An early study of Claußnitzer and Névir (2009) suggests that mid and upper troposphere vorticity advection can also play a role in convection initation and can determine its strength. This is partly confirmed by a study of Weijenborg *et al.* (2015), but requires further extensive evaluation. Upper–mid-level static instability, as evidenced by tropospheric quantities such as convection triggering potential (CTP), analogous to convective available potential energy (CAPE), and dew-point depressions, can also play a considerable role in constraining moist convection, even when locally forced by the land surface (e.g., Findell and Eltahir, 2003a; 2003b).

Figure 3 shows the three-month mean cloud liquid water path (LWP) derived from the CM SAF CLoud property dAtAset using the Spinning Enhanced Visible and InfraRed Imager (SEVIRI) Edition 2 (CLAAS2) data set (Finkensieper *et al.* 2016b). High values of LWP are observed over the mountains, confirming the convergence zones shown in Figure 2. Further details about this product are explained in section 4.

Figure 4 shows the accumulated precipitation during summer 2015 as derived from CHRIPS V2 (Funk *et al.* 2015). The precipitation maximum over the Al Hajar mountain region is clearly visible, with a maximum reaching 15 mm throughout the summer. This is consistent with findings of Sherif *et al.* (2014), who investigated annual precipitation patterns over four different regions in the UAE.

3 | WRF MODEL DESIGN AND SETUP

The model ensemble is based on the Weather Research and Forecasting model (WRF: Skamarock *et al.*, 2008) version 3.8.1, together with the Advanced Research WRF (ARW) core. The ARW core solves the Euler equations on a discretized horizontal grid with terrain-following vertical coordinates.

For simulating the convection and convective initiation and thus seedable clouds, it is important to apply a high horizontal model resolution in order to represent convergence zones, especially over the mountains (Schwitalla *et al.* 2008; Bennett *et al.* 2011; Wulfmeyer *et al.* 2011), which is the prevailing situation over the UAE during summer time. Therefore it is necessary to operate the model on the CP scale, which corresponds to grid increments < 4 km (Bauer *et al.* 2011; 2015; Schwitalla *et al.* 2011; 2017).

The selected model domain comprises 900×700 grid cells in the horizontal direction and 100 vertical levels. In the lowest 2,000 m above ground, the level density is increased so that ∼25 levels are present, in order to be able to resolve the strong moisture gradients in the planetary boundary layer and the lower troposphere. All simulations were performed with a CP horizontal grid increment of 0.025° (≈2,779 m). No parametrization of deep convection was applied. Soil texture data are obtained from Milovac

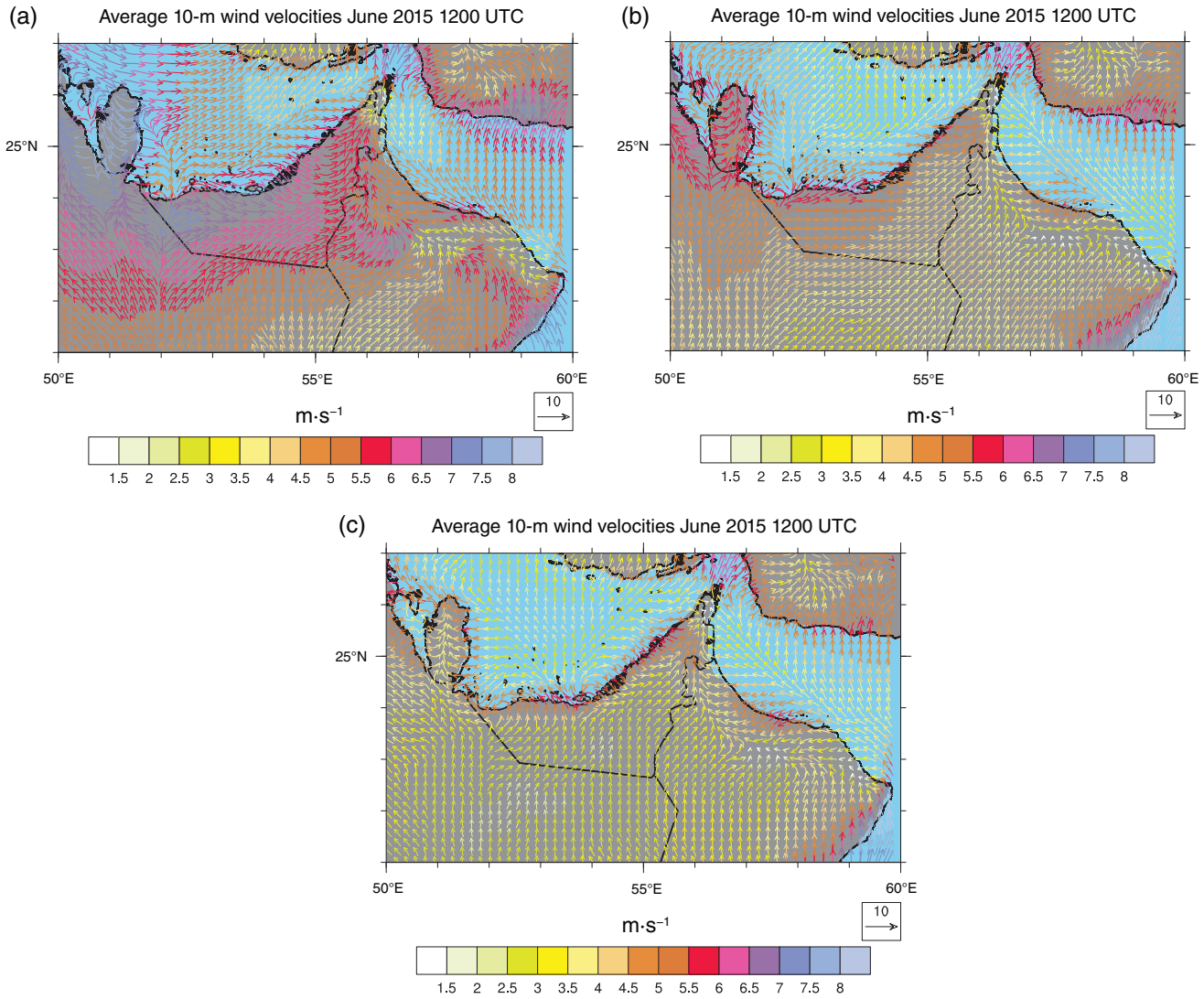

FIGURE 2 ECMWF operational analysis 10-m wind velocities averaged over June, July, and August 2015 for 1200 UTC

et al. (2014) and a high-resolution land-use data set for the UAE was provided by the National Center for Meteorology (NCM) in Abu Dhabi. The data were reclassified from the original categories to the 20 class IGBP–MODIS categories applied in WRF. The model domain and applied land-cover data over the eastern UAE are shown in Figure 5a,b. The model was compiled with the Intel compiler version 18 and the simulations were performed on the Cray XC40 system at the High-Performance Computing Center Stuttgart (HLRS).

Initial and boundary conditions were obtained from the operational ECMWF IFS operational forecasting system cycle 41r1. The horizontal resolution is approx. 16 km, with 137 levels up to 0.01 hPa, and 100 levels being available until the applied model top of 20 hPa. In addition to the ECMWF data, high-resolution sea-surface temperature (SST) data from the Operational Sea Surface Temperature and Ice Analysis (OSTIA) project (Donlon *et al.* 2012) were used, providing a better representation of near-coastal areas. Soil moisture and temperatures are obtained from the ECMWF analyses, which assimilate satellite soil-moisture data (Albergel *et al.* 2012) into the ECMWF land-surface model HTESSEL (Balsamo *et al.* 2009). An initial comparison revealed no major differences between the ECMWF and WRF soil moisture, as the soil moisture is very low, with values less than 0.1 $m^3 \cdot m^{-3}$. Nevertheless, a four-week soil-moisture spin-up simulation was performed to avoid inconsistencies. The simulation period is 18 hr, as the main interest is in convective activity during the daytime.

Additionally, all members make use of the aerosol optical depth data from the ECMWF Composition and Climate atmospheric composition and climate reanalysis project (Inness *et al.* 2013) interacting with the shortwave radiation scheme.

Land-surface processes and land–atmosphere interaction were represented by the Noah LSM with multi-parameterization options (NOAH-MP) land-surface

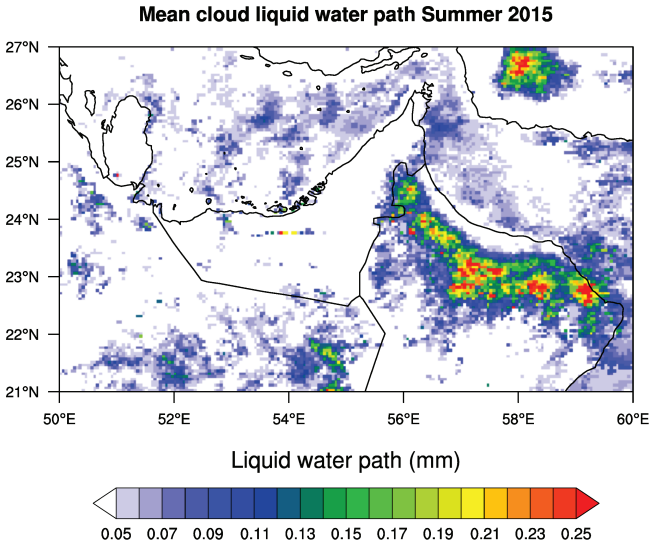

FIGURE 3 Mean cloud liquid water path from the CLAAS 2 data set during summer 2015

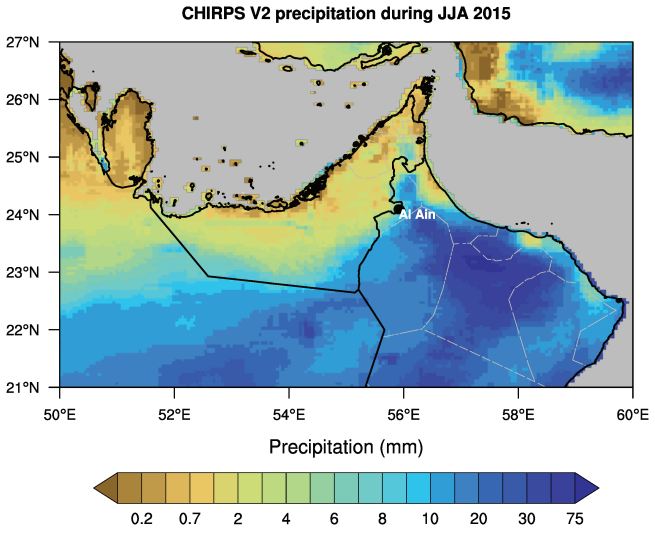

FIGURE 4 CHIRPS V2 accumulated precipitation during summer 2015

model (LSM; Niu *et al.*, 2011). Compared with the more simple NOAH LSM (Ek *et al.* 2003), NOAH-MP contains a separate vegetation canopy defined by a canopy top and bottom layer including a modified energy-balance closure approach. It allows for dynamic vegetation and different approaches for radiation budget calculation. NOAH-MP also contains a tile approach, where the net longwave radiation and turbulent fluxes are calculated separately for bare soil and the canopy layer. The calculated fluxes over canopy grid cells are a weighted sum of canopy and bare soil fluxes. Further details about the differences between NOAH and NOAH-MP and the selected NOAH-MP options applied in this study can be found in Milovac *et al.* (2016).

Please note that a most accurate consideration of land cover such as vegetation was not that important for these ensemble simulations, but was for the second OCAL objective. The study of land-cover modifications such as plantations for the enhancement of cloud and precipitation development requires a consistent model system with an up-to-date data set.

In contrast to the NOAH LSM, the turbulent exchange parameters over land used by the planetary boundary layer (PBL) schemes are calculated directly in NOAH-MP instead of the surface-layer scheme (Nielsen, 2013). Over water areas, the MM5 surface-layer scheme (Jimenéz *et al.* 2012) calculates all turbulent fluxes.

To represent the interaction of the land surface with atmospheric variables like temperature, moisture, clouds, and wind, the Mellor–Yamada–Nakanishi–Niino (MYNN) PBL parametrization (Nakanishi and Niino, 2006) coupled with the MYNN surface-layer scheme is applied. The MYNN PBL is being evaluated extensively in the WRF community (e.g., Shin and Hong, 2011; Chaouch *et al.* 2017; Fekih and Mohamed, 2017). MYNN is a local approach based on the level 1.5 turbulent kinetic energy (TKE) closure scheme of Mellor and Yamada (1974), in which the turbulent fluxes of any conserved quantity are related to gradients of their mean values at adjacent levels only. The height of the PBL (PBLH) is diagnosed based on a weighted sum of the calculation of PBLH from the vertical profile of potential temperature and PBLH calculated from TKE.

Radiation is parametrized by the Rapid Radiative Transfer Model for Global Circulations Models (RRTMG: Iacono *et al.*, 2008) for shortwave and longwave radiation. This scheme is a highly efficient parametrization and is widely used in the WRF and numerical weather prediction (NWP) community (Branch *et al.* 2014; Schwitalla *et al.* 2017; Strobach and Bel, 2019). RRTMG has 14 wavebands for shortwave and 16 bands for longwave radiation and accounts for the absorption of atmospheric gases like CO_2, N_2O, and CH_4. It also contains a subgrid-scale cloud module based on fractional cloud cover and interacts with cloud microphysical properties like cloud water, cloud ice, snow, and rain water. The CO_2 content is set to 395 ppm in our study.

Cloud microphysics is represented by the scheme of Thompson *et al.* (2008). This scheme is a double-moment scheme predicting mass mixing ratios of cloud water, rain water, cloud ice, snow, and graupel, as well as the number concentrations of cloud ice and rain. As the developer suggested increasing the number of cloud droplets from $100\times10^6\ m^{-3}$ to a higher value, this value was increased to $200\times10^6\ m^{-3}$, which is considered as an intermediate aerosol loading, although this can lead to a reduction of

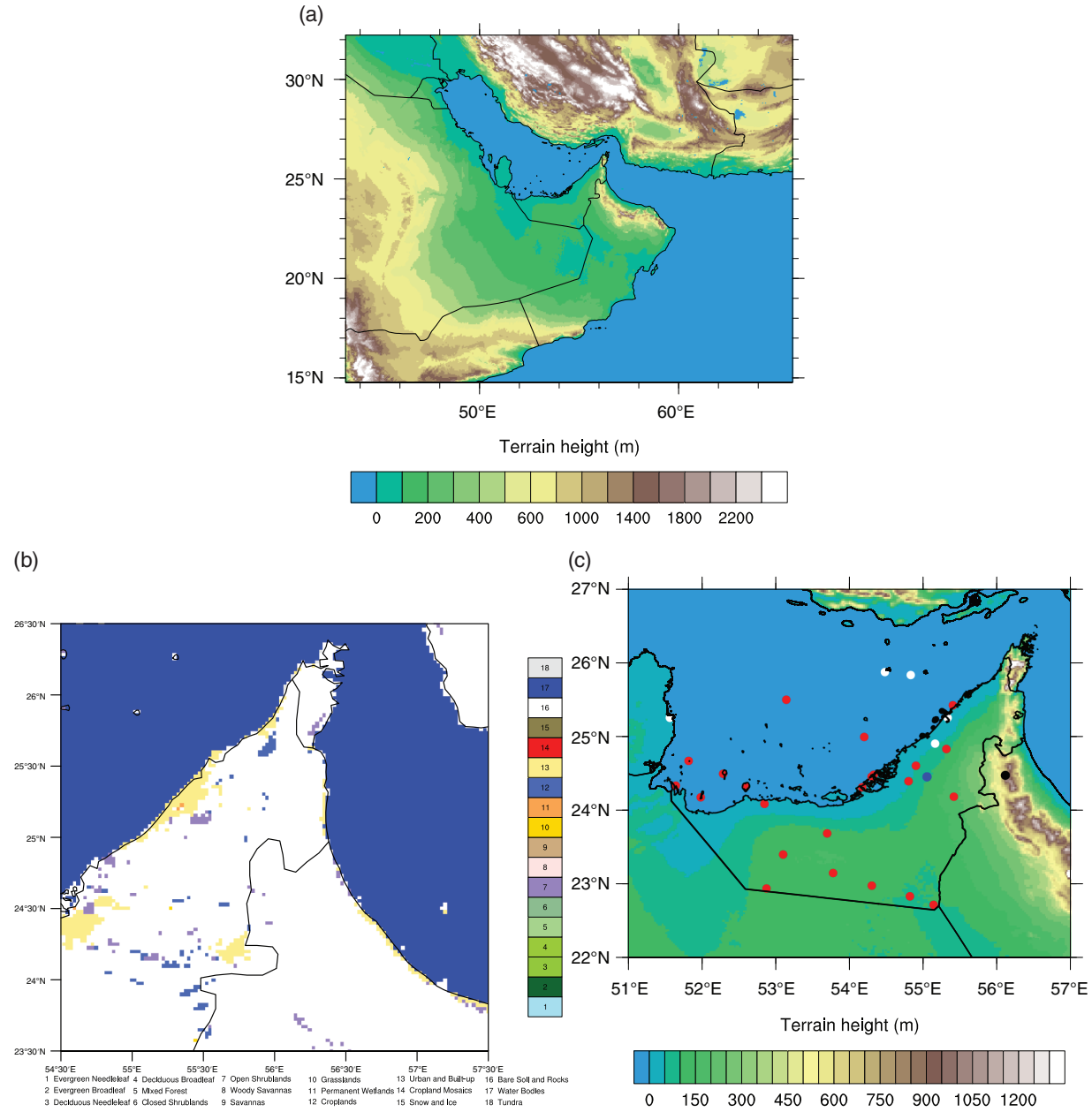

FIGURE 5 (a) Map of the applied WRF model domain with terrain height. (b) Landcover data zoom over the eastern UAE. (c) Zoom into the UAE with the surface stations from NCM (red dots) and GTS (white dots) used for validation. The black and blue dots denotes the locations for the time series shown in section

rain due to nonlinear effects (Khain *et al.* 2009; Heikenfeld *et al.* 2019).

As even a CP resolution of 0.025° can still be too coarse to represent shallow clouds (Prein *et al.* 2015; Kendon *et al.* 2017), the global and regional integrated model system (GRIMs) shallow convection scheme (Hong *et al.* 2013) is applied, as this scheme can be used independently of other parametrizations.

To investigate the simulated cloud and precipitation development sensitivity with respect to the applied model physics, the choice of PBL parametrization and cloud microphysics was varied.

The MYNN PBL scheme was replaced by the Yonsei University (YSU) PBL parametrization (Hong *et al.* 2006; Hong, 2007). The YSU PBL scheme is a nonlocal approach, where large eddies are taken into account by adding a countergradient correction term to the turbulent fluxes. The reader should note that the GRIMs shallow convection scheme has an additional interaction with the YSU scheme via the entrainment layer depth calculated in the YSU scheme.

Argüeso *et al.* (2011), García-Díez *et al.* (2013), and Steeneveld *et al.* (2015) investigated the performance of different PBL schemes over different regions. Their studies

TABLE 1 Parametrizations used in the five-member ensemble

Experiment name	Microphysics	PBL scheme	Surface layer physics	Aerosol climatology
CONTROL	Thompson 2-moment (Thompson *et al.* 2008)	MYNN (Nakanishi and Niino, 2006)	MYNN	Tegen *et al.* (1997)
AERO	Thompson aerosol-aware (Thompson and Eidhammer, 2014)	MYNN	MYNN	Colarco *et al.* (2010)
AERO_YSU	Thompson aerosol-aware (Thompson and Eidhammer, 2014)	YSU (Hong, 2007)	MM5 (Jimenéz *et al.* 2012)	Colarco *et al.* (2010)
N_AERO_YSU	Thompson 2-moment (Thompson *et al.* 2008)	YSU	MM5	Tegen *et al.* (1997)
WDM6	WDM6 (Lim and Hong, 2010)	MYNN	MYNN	Tegen *et al.* (1997)

show that the results often depend on the evaluation region. Chaouch *et al.* (2017) investigated the performance of different PBL parametrizations over the Arabian Peninsula and found the best performance for nonlocal schemes, although a negative near-surface dewpoint bias is present with all applied PBL schemes.

The cloud microphysics was switched from the Thompson scheme without aerosol considerations to the Thompson aerosol-aware scheme of Thompson and Eidhammer (2014). The aerosol climatology for the Thompson aerosol-aware scheme is provided on the WRF web page based on the work of Colarco *et al.* (2010) and is converted to number concentration ratios to be used in WRF. The aerosol-aware scheme is expected to improve cloud properties by a direct coupling to the RRTMG radiation scheme (Thompson *et al.* 2016). Additionally, the double-moment 6-class microphysics scheme (WDM6) microphysics scheme of Lim and Hong (2010) is applied. WDM6 is also a double-moment scheme with prognostic equations for the same hydrometeors as the Thompson scheme, but includes a prognostic equation for the cloud droplet concentration, which is prescribed in the non-aerosol aware Thompson scheme. This scheme is also widely used in the WRF community (Bae *et al.* 2016; Galligani *et al.* 2017; Song and Sohn, 2018). Keep in mind that WDM6 does not interact with aerosol data like the Thompson aerosol-aware scheme.

Table 1 summarizes the applied parametrizations and options for the five-member physics ensemble.

4 | VALIDATION DATA SETS

For validation, surface stations and satellite data are applied. To achieve a higher station density over the UAE, compared with data from the global telecommunication system (GTS), additional surface observations were provided by the UAE NCM. The data were quality-controlled by NCM staff prior to the data provision. The overall station distribution is shown in Figure 5c. In our study, we focus on the 2-m temperature, 2-m humidity, and 10-m wind velocities for the part of the UAE west of 55.5°E. Surface stations in the eastern part of the UAE are not considered for evaluation, as they are often located in small towns not represented by the model and thus show a heat-island effect during night-time, to the disadvantage of model performance.

In addition, the shortwave downward radiation product from the *EUMETSAT* Satellite Application Facility on Land Surface Analysis (LSA SAF: Trigo *et al.*, 2011) is applied. This data set provides instantaneous downwelling shortwave downward radiation flux measurements (*SWDOWN*) from the *Meteosat* Second Generation (MSG) SEVIRI instruments over the wavelength interval between 0.4 and 4 μm at a spatial resolution of 0.05° × 0.05° with a temporal resolution of 30 min. The *SWDOWN* product has an accuracy of 10% for the case in which *SWDOWN* is larger than 200 $W \cdot m^{-2}$ and an accuracy of 20 $W \cdot m^{-2}$ otherwise.

In order to investigate the cloud evolution, we applied the Satellite Application Facility on Climate Monitoring CLoud property dAtAset using SEVIRI–Edition 2 (CM–SAF CLAAS2) data set (Finkensieper *et al.* 2016b), providing information about the cloud liquid water path (*CWP*) during daylight. This product provides information on cloud properties derived from the 0.6-, 0.8-, and 1.6-μm channels of the MSG SEVIRI instrument. The ground resolution over the Arabian Peninsula is about 5 km and the data are available every 15 min at a 0.05° × 0.05° resolution.

According to the validation report (Finkensieper *et al.* 2016a), the accuracy of the *CWP* product is 10 g·m^{-2}. As *CWP* is derived from optical depth data using the relation from Stephens (1978) depending on optical depth, we discard all observations showing *CWP* values less than 0.05 mm (Kniffka *et al.* 2014).

Validation of precipitation is performed against the Climate Hazards Group Infrared Precipitation with station data (CHIRPS; Funk *et al.*, 2015). The data set is based on the TRMM Multi-Satellite precipitation analysis 3B42 product (NASA, 2011). The satellite data are blended with available surface observations based on a sophisticated inverse distance weighting algorithm. This data set is available on a 3 hr to monthly basis at a horizontal resolution of 0.05° between 50°N and 50°S. In our study, the daily product was applied.

The statistics for 2-m temperatures and dewpoints as well as 10-m wind speeds are obtained with the Model Evaluation Tool (MET) developed by the Developmental Testbed Center (DTC, 2017). Model grid points were interpolated to the NCM weather station locations by using a 3×3 distance-weighted mean of the surrounding model grid boxes.

5 | CASE STUDY DESCRIPTION

After the set up of our model system, we performed our case study for July 14, 2015. This day was chosen as it represents a typical weather situation over the UAE. The day started without any single cloud over land and was characterized by a midtroposphere low-pressure system centered over the eastern part of Saudi Arabia, associated with a surface heat low-pressure system (upper panel of Figure 6). Mid- and upper-level winds over the eastern part of the Arabian Peninsula are coming from the east, associated with a strong wind shear in the upper troposphere, indicated by the different wind directions at 500 and 300 hPa (not shown).

In the lower troposphere at 925 hPa, the wind directions show large variability, with a southerly flow over the UAE (lower panel of Figure 6). The water-vapor mixing ratios over the Arabian Peninsula are found to be between 5 and 17 g·kg^{-1}. The 850-hPa temperatures reached 30°, resulting in 2-m temperatures of more than 45° during the day. Together with very high water temperatures of more than 30° and thus a very high moisture content in the Arabian Gulf, this results in very high values of CAPE of more than 1500 J·kg^{-1} over the sea and near the coasts (not shown).

These meteorological conditions result in convection initiation over the Al Hajar Mountain range, with a level of free convection (*LFC*) around 550 hPa and isolated precipitation in this area.

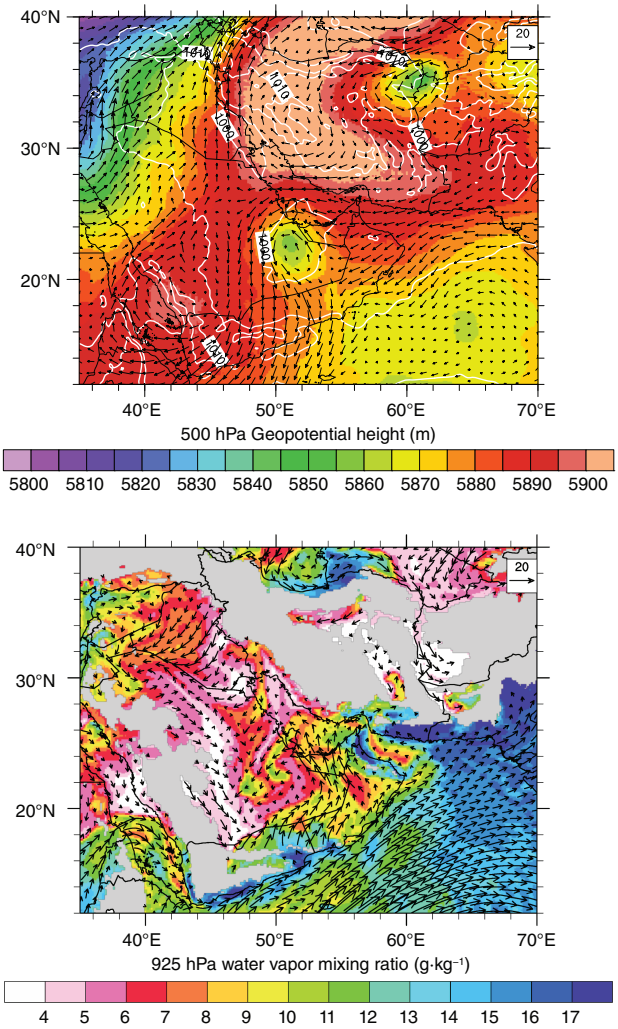

FIGURE 6 Upper panel: 500 hPa geopotential height (shaded) with overlaid wind vectors (m·s^{-1}) and sea-level pressure contour lines (hPa) for July 14, 2015 0600 UTC. Lower panel: 925 hPa water-vapor mixing ratios (shaded) with wind vectors (m·s^{-1}). Data are obtained from the operational ECMWF analysis. Gray areas denote regions above 925 hPa

6 | RESULTS

6.1 | Surface radiation

Figure 7 shows a comparison of the mean LSA SAF *SWDOWN* with the mean *SWDOWN* values of the AERO, AERO_YSU, CONTROL, and WDM6 simulations over the simulation domain. The data are available every 15 min and averaged between 1000 UTC and 1300 UTC, which is the time period where the main convection occurs.

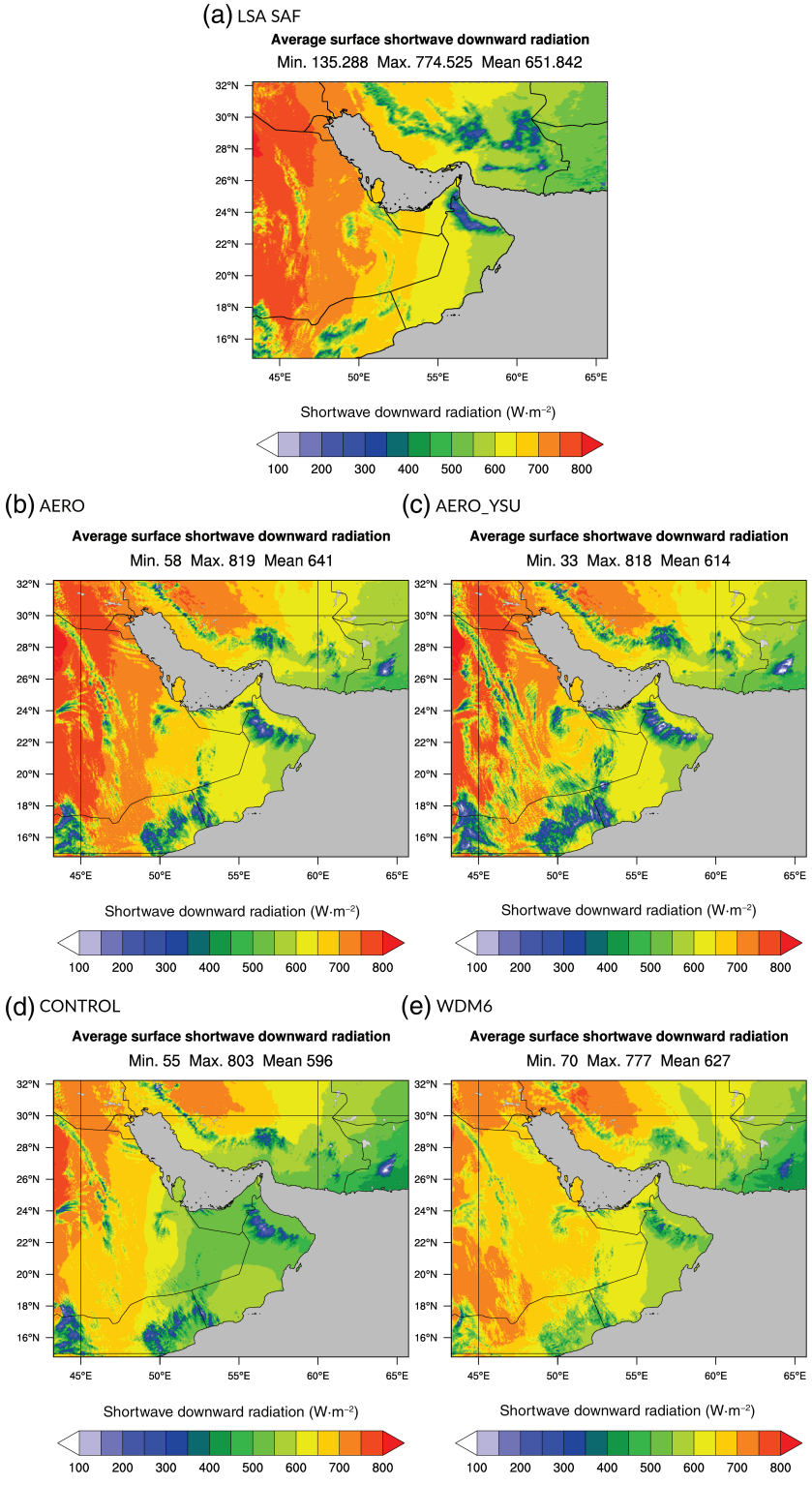

FIGURE 7 Mean *SWDOWN* flux of (a) LSA SAF product, (b) AERO simulation, (c) AERO_YSU, (d) CONTROL, and (e) WDM6 simulation. The data are averaged between 1000 and 1300 UTC

The LSA SAF *SWDOWN* flux observation shows a west–east gradient between 800 and 500 $W \cdot m^{-2}$. The cloud development over the Al Hajar mountains is clearly visible, with values of less than 300 $W \cdot m^{-2}$, as well as the mid- and low-level clouds associated with the low-pressure system over Saudi Arabia. The AERO simulation (Figure 7b) shows a similar cloud pattern over the Al Hajar mountains, with values less than 300 $W \cdot m^{-2}$. The AERO_YSU simulation tends to overestimate the cloud coverage, especially in the southern part of the model domain, and also shows a more frequent occurrence of shallow clouds in the western half of the model domain.

The CONTROL simulation (Figure 7d) shows a similar cloud pattern to the AERO simulation, but the absolute

values of *SWDOWN* are less than in the simulation with the aerosol-aware Thompson scheme. The WDM6 simulation simulates considerably less cloud coverage compared with all other simulations.

The mean observed *SWDOWN* flux is 651 $W \cdot m^{-2}$, while the simulated values are 597, 642, 614, and 627 $W \cdot m^{-2}$ for the CONTROL, AERO, AERO_YSU, and WDM6 simulations, respectively.

It is interesting to note that the *SWDOWN* flux minimum is less in all of the simulations, with AERO_YSU showing the lowest value of 33 $W \cdot m^{-2}$. The standard deviations of nearly all model simulations are higher than observed, especially the AERO_YSU simulation, which shows a value of 120 $W \cdot m^{-2}$, while the observation has a standard deviation of 95 $W \cdot m^{-2}$.

Although the mean value only shows a difference of 5%, this points to more deeper and more localized clouds in the simulation. In contrast, the WDM6 shows a standard deviation of 75 $W \cdot m^{-2}$, pointing to an underestimation of cloud development. This is confirmed by the *CWP* shown later (in Figure 12e).

Compared with the default applied aerosol climatology of Tegen *et al.* (1997) for the CONTROL, N_AERO_YSU, and WDM6 simulations, application of the water- and ice-friendly aerosol climatology of Colarco *et al.* (2010) helps to improve the shortwave irradiation.

6.2 | Surface variables

Figure 8a shows the mean diurnal cycle of 2-m temperature averaged over the western part of the UAE up to 55.5°E. The available stations are shown by the red dots in Figure 5c. It is seen that the initial state mean at 0000 UTC is in perfect agreement with the observations.

During the morning transition until 0400 UTC (8:00 a.m. local time), all model simulations show a moderate cold bias of about 4 K, which reduces to almost zero during daytime. During the evening transition after 1400 UTC, all simulations show a cold bias of 3 K. It is interesting to note here that stations located in the inland desert region show a stronger temperature bias compared with stations near the coast. The root-mean-square error (RMSE) increases to around 4.5 K during the morning and evening transition, while it is around 3 K during the daytime. The correlation drops down to almost zero during these periods, while it increases to 0.97 during the daytime.

For the mean 2-m dewpoints (Figure 8b), all simulations show a negative bias of 2 K during the morning transition, turning into a positive bias of 3 K during daytime and matching the observations after 1200 UTC, and the correlations remain above 0.9 (not shown).

Figure 8c shows the diurnal cycle of the 10-m wind speeds for the western part of the UAE. All simulations follow the observed diurnal cycle. During daytime, the simulations show a positive bias of 1.5 $m \cdot s^{-1}$, turning into a negative bias after sunset.

6.3 | Vertical distribution of temperature and moisture

To complement the evaluation of shortwave radiation, 2-m temperatures, and 2-m dewpoints, the vertical structures of moisture were investigated. Figure 9 shows a time series of moisture over the mountains (upper two rows) and the desert (lower two rows). The locations are shown by the black and blue dots in Figure 5c. From Figure 9a,b, we see that both the YSU and MYNN PBL schemes simulate similar boundary-layer heights of up to 5000 m above ground level (AGL) over the mountains northeast of Al Ain. These values were confirmed by the sounding of Abu Dhabi International Airport.

At 0430 and 0900 UTC, both experiments show a moist plume over the mountain, expanding from the surface to about 1,500 m AGL. This is related to moist air masses advected from the Gulf of Oman reaching the mountain tops. The AERO simulation shows higher values of water vapor, probably as a result of stronger mixing inside the PBL, although the updrafts are weaker by 0.5 $m \cdot s^{-1}$ (not shown).

In the further course of the day, the MYNN PBL simulates higher horizontal wind speeds compared with the YSU PBL, resulting in a stronger convergence at higher altitudes over the mountain at 0900 UTC (1:00 p.m. local time). This is also seen by strong updraft velocities exceeding 4 $m \cdot s^{-1}$ followed by strong downdrafts of more than 4 $m \cdot s^{-1}$ throughout the atmosphere, associated with rain reaching the ground and stabilizing the atmosphere, as seen by the gradient Richardson number *Ri* (Chan, 2008; Figure 10a). Further, another moist plume starts to rise around 1300 UTC in both experiments, with higher moisture values in the AERO_YSU simulation, as the wind direction in both simulations shows a northerly component.

The AERO_YSU simulation only shows a very weak convergence at higher altitudes and also does not simulate any rain water. At 1330 UTC, the AERO simulation shows another convergence zone with moist air rising from the ground, while the AERO_YSU simulation shows a strong convergence with moderate updrafts, leading to cloud formation but without any rain, also reflected in the gradient Richardson number *Ri* (Figure 10b). It is also worth noting that the simulation with the MYNN PBL scheme starts

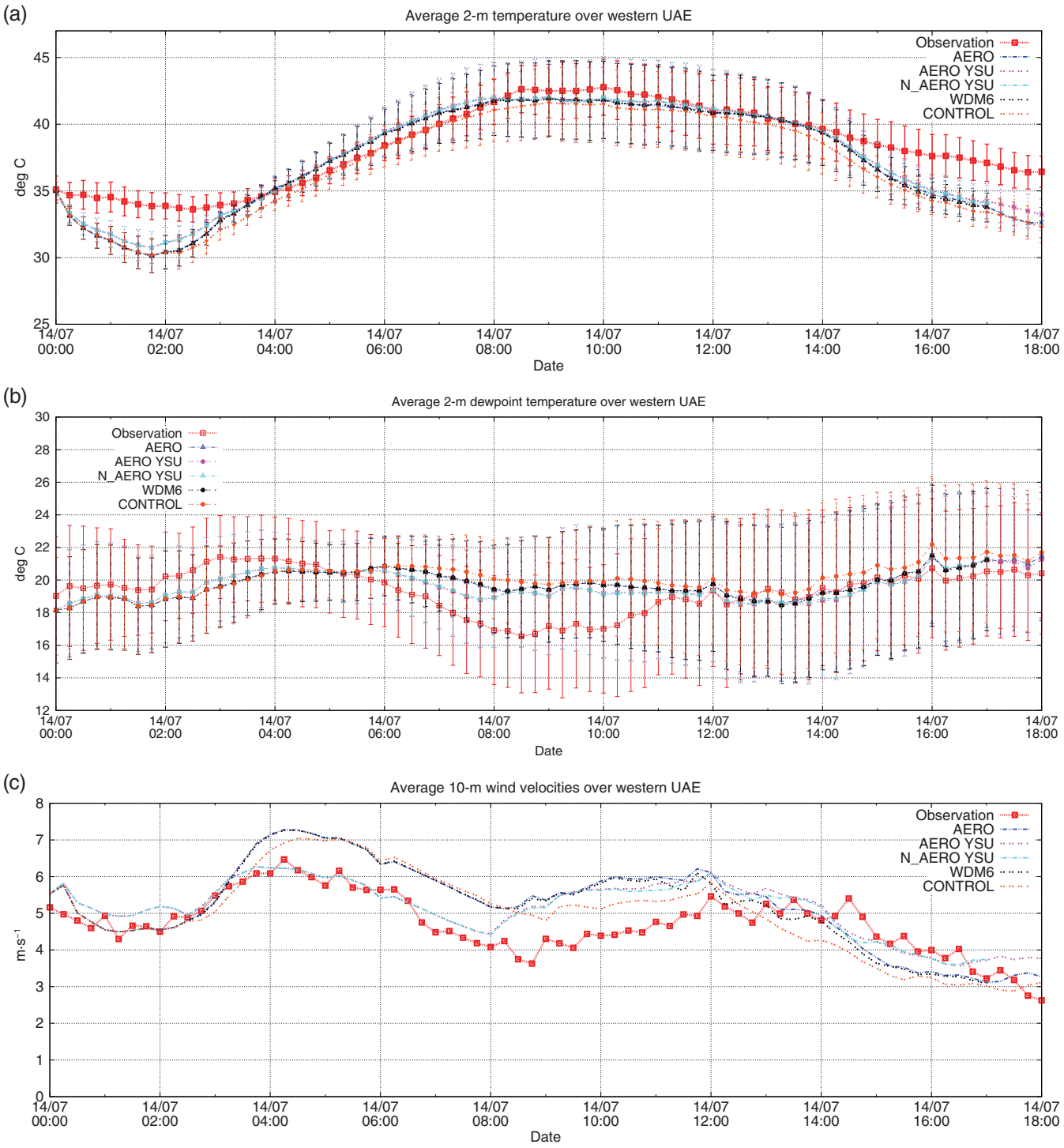

FIGURE 8 Mean diurnal cycle of (a) 2-m temperature, (b) 2-m dewpoint, and (c) 10-m wind speeds averaged over the western UAE up to 55.5°E

to spin up turbulence earlier than the simulation with the YSU PBL scheme.

For the desert location (Figure 9c,d), the southerly low-level jet originating from the Arabian Sea and Oman is clearly visible up to 1,000 m ASL until 0645 UTC, followed by a strong weakening of the the low-level winds (Ranjha *et al.* 2015). The large amount of near-surface moisture is transported to higher altitudes during the day as the boundary layer starts to evolve. At 1115 UTC, stronger updrafts occur in the AERO simulation (not shown here) and additional moisture is transferred to the lower troposphere, followed by a convergence line up

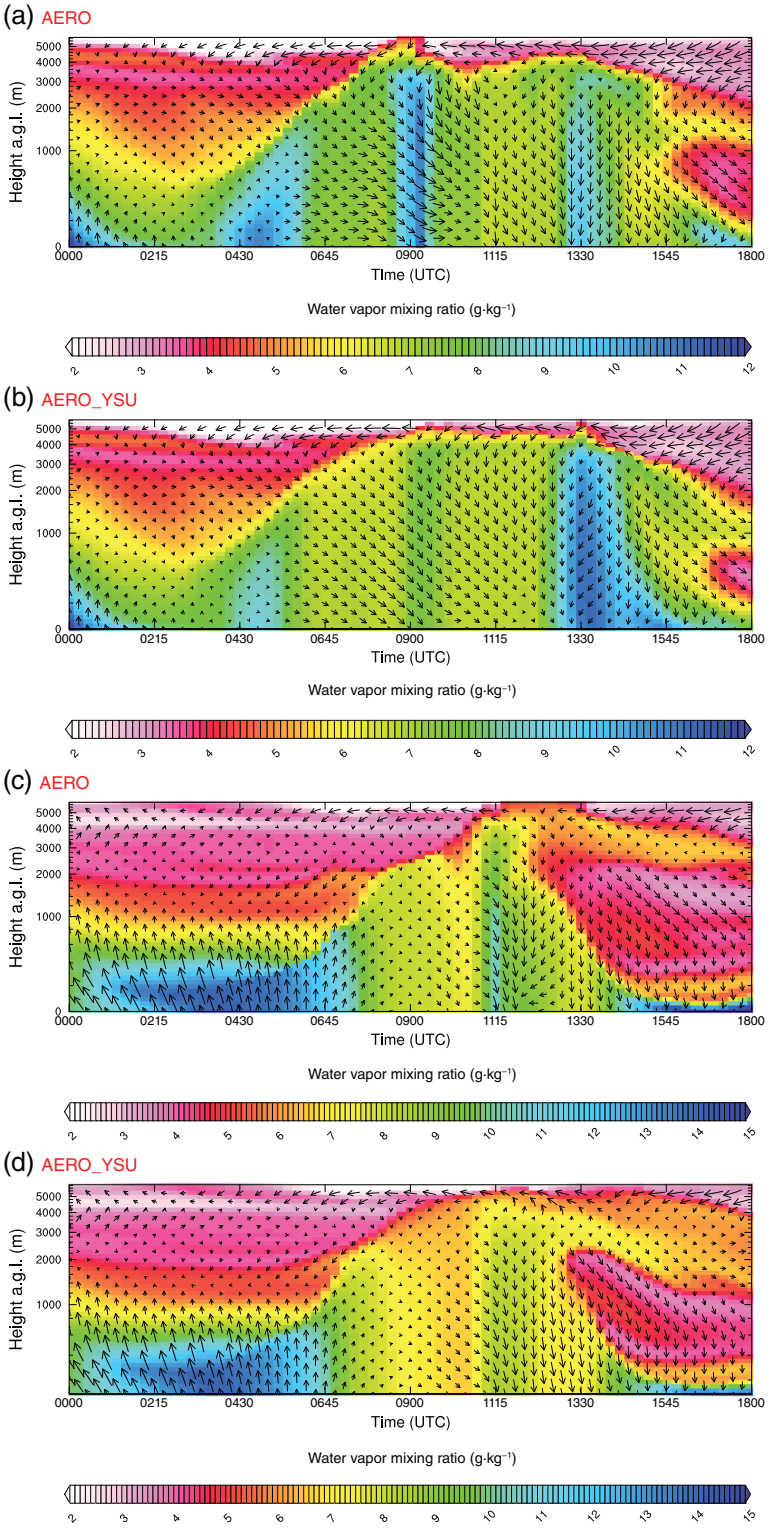

FIGURE 9 Time series of water vapor (together with horizontal wind vectors in black) for (a,b) a grid cell close to Al Ain and (c,d) a desert grid cell west of Al Ain. The locations are denoted in Figure 5c and the temporal resolution is 15 min

to 2,000 m ASL, which is not visible in the AERO_YSU simulation. The sudden drying between 500 and 2,500 m AGL is caused by a northwesterly flow carrying overlying drier air masses from the Arabian Gulf toward the desert, overcompensating for the southerly flow from the Saudi Arabian heat low.

Currently it is difficult to evaluate the quality of the vertical structures of temperature, moisture, and wind due to the unavailability of high spatial and temporal resolution atmospheric profiler data like differential absorption lidar and Raman lidar instrumentation (Hammann *et al.* 2015; Späth *et al.* 2016).

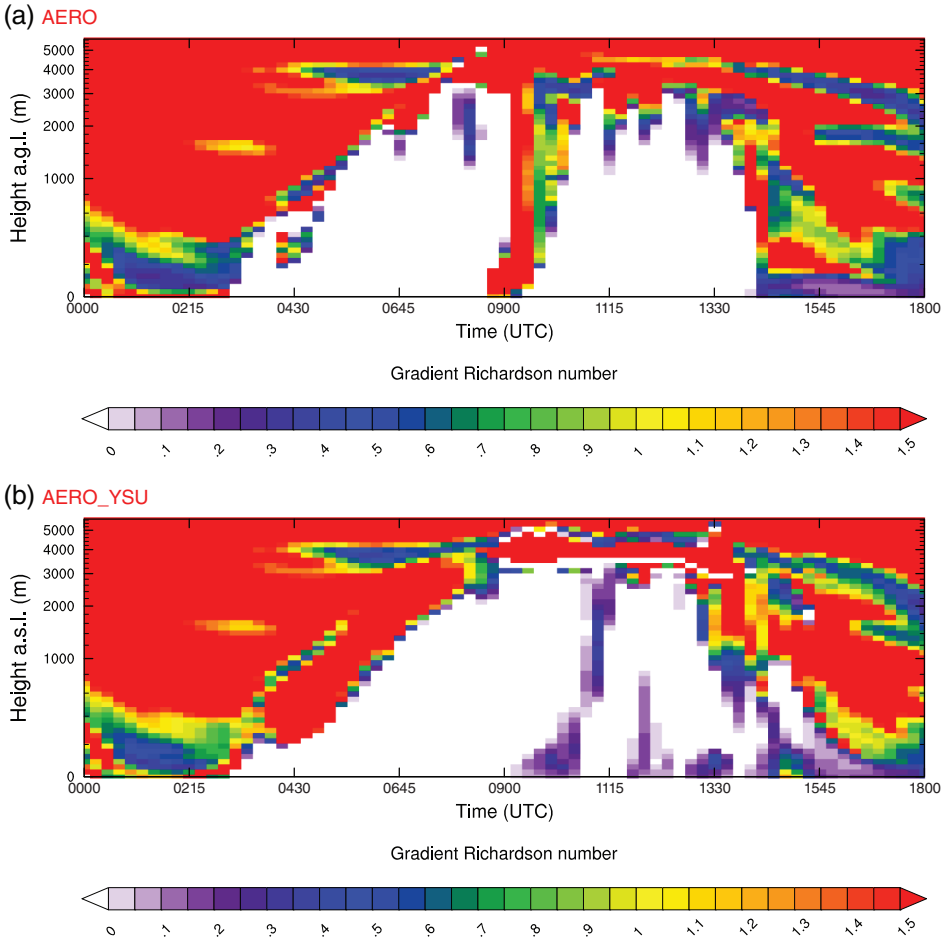

FIGURE 10 Similar to Figure 9a,b, but for the gradient Richardson number *Ri*. White areas indicate turbulence regions

6.4 | *CAPE* and *CIN*

Additionally, the mean values of Convective Available Potential Energy (*CAPE*) and Convective Inhibition (*CIN*) were investigated. Figure 11, as an example, shows the averaged most unstable *CAPE* (*CAPE_MU*) and *CIN* (*CIN_MU*) values over the UAE and Al Hajar mountains between 0600 and 0945 UTC for the AERO and AERO_YSU simulations. This time period was chosen, as it shows the situation before and at the beginning of convective activities. *MU_CAPE* and *MU_CIN* are based on a particle ascending from the most unstable model level from the lowest 180 hPa above ground, i.e. the parcel with maximum buoyancy is used for the *CAPE* calculation.

The mean *CAPE* value of the AERO simulation averaged over the domain shown in Figure 11a is 90 J·kg $^{-1}$ higher than that in the AERO_YSU simulation (439 J·kg $^{-1}$), while at the same time the *CIN* of the AERO simulation is around 40 J·kg $^{-1}$ lower than that in the AERO_YSU simulation (193 J·kg $^{-1}$). The differences are most pronounced over the desert regions of Oman and the UAE. This points toward a more stable atmospheric stratification in the AERO_YSU simulation and thus a stronger inhibition of convection reflected in the time–height cross-sections shown in Figure 9 and the precipitation patterns shown later (in Figure 15).

A brief comparison with the MSG-derived global instability index at various time steps revealed an underestimation of the particle lifted index (*LI*: Blanchard, 1998), mainly over the eastern UAE desert, compared with the WRF simulations. The *Meteosat* satellite data product indicates a *LI* of less than −6 K, whereas AERO and AERO_YSU simulate more stable *LI* values of around −3 K.

6.5 | Cloud development

To study the cloud development, the WRF simulations were compared with *CWP* observations provided by CLAAS. Figure 12 shows frequency histograms between 0600 and 1300 UTC of the CONTROL, AERO, AERO_YSU, and WDM6 simulations compared with the CLAAS observations. Data are averaged between 21°N–26.8°N and 53.8°E–59.5°E. Please keep in mind that *CWP* observations are only available during daylight.

Compared with the CM–SAF observation, the WDM6 simulations shows the least cloud liquid water path, while

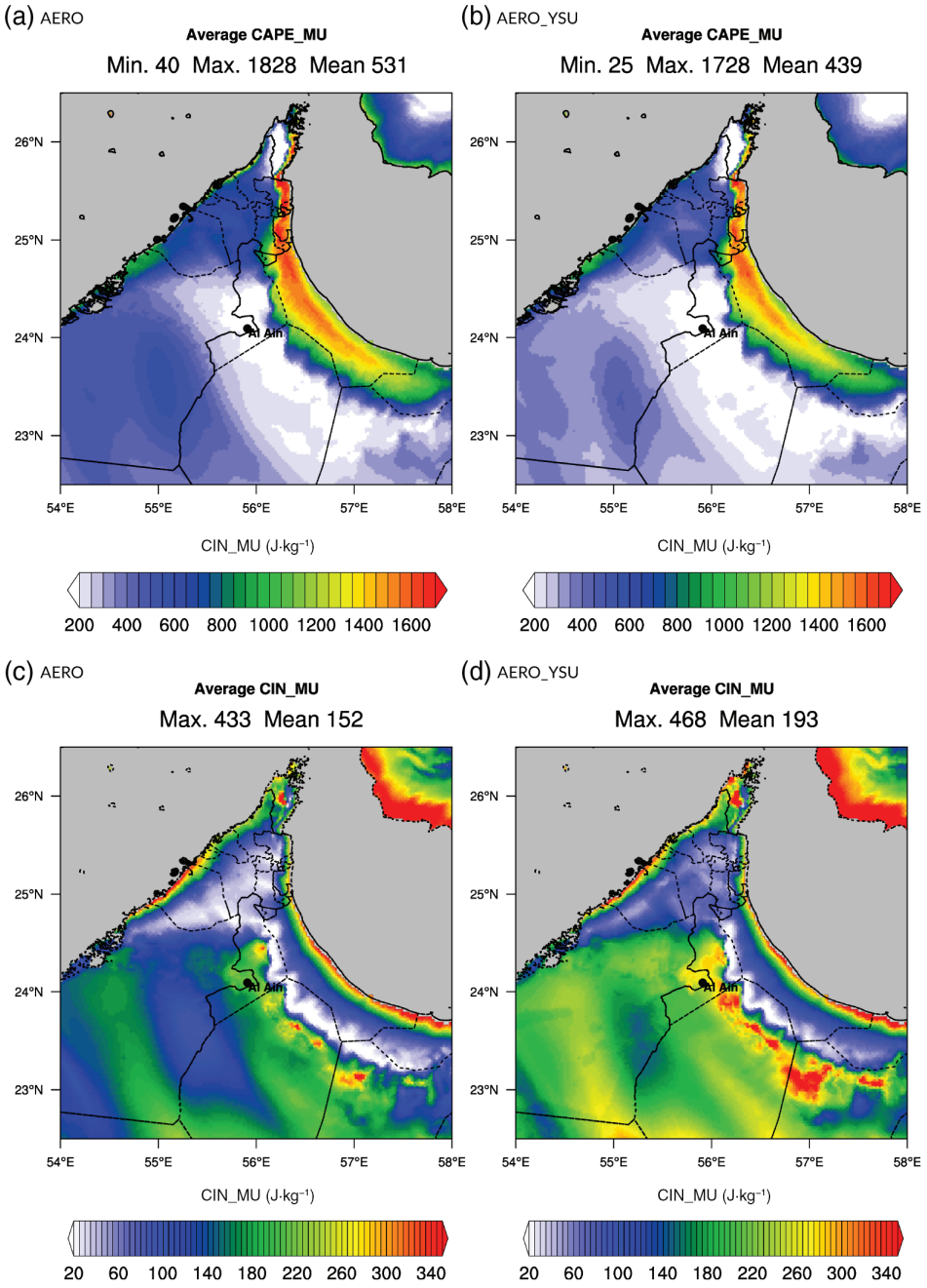

FIGURE 11 Mean *CAPE* (upper row) and *CIN* (lower row) between 0600 and 0945 UTC. Left column: AERO simulation. Right column: AERO_YSU simulation

the CONTROL experiment simulates more clouds inside the model domain. For the case in which aerosol climatologies are included and the aerosol-aware Thompson scheme (Thompson and Eidhammer, 2014) is applied, the distribution is closer to the observed distribution. If the MYNN PBL scheme is replaced by the YSU PBL scheme, the model simulation is even closer to the observation in terms of cloud liquid water. In contrast to the simulation with the Thompson scheme, the WDM6 microphysics generates too many ice clouds at higher altitudes, which do not transform into precipitation.

All simulations start to develop clouds after 0700 UTC over the Al Hajar mountains (Figure 13). The further diurnal cycle is well captured by all experiments, while the amount of cloud liquid water is overestimated in all simulations. During the afternoon, the observed cloud water amount is higher than simulated, with the WDM6 simulation showing the least cloud water amount. The highest values of the AERO simulation between 1000 and 1100 UTC can be related to strong isolated precipitation events (see later in Figure 15c). Although the WDM6 simulation shows the least *CWP* content over the UAE and Al Hajar mountains (Figure 12), two isolated cloud cells with very high *CWP* values are simulated, increasing the mean *CWP* between 0800 and 1100 UTC.

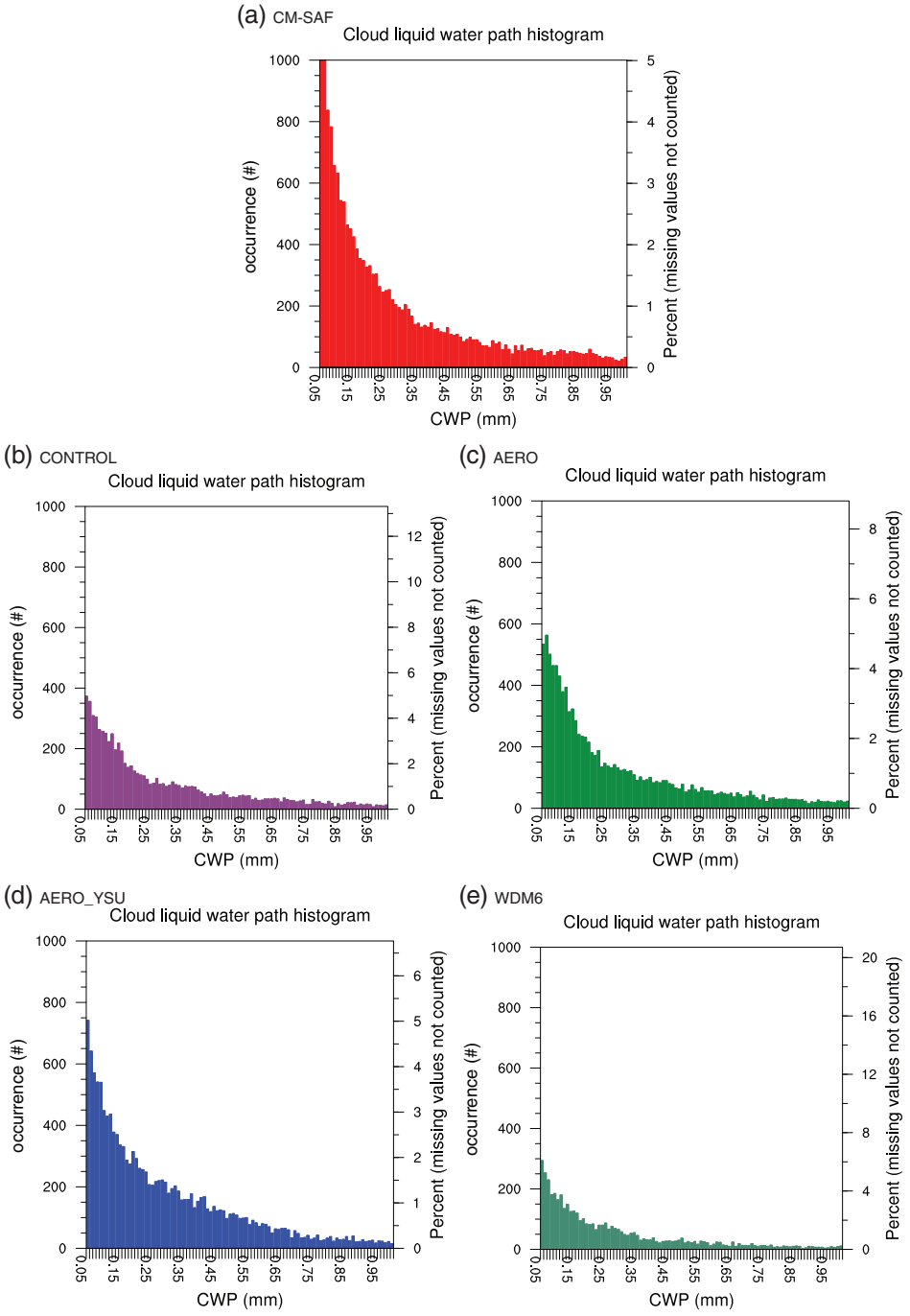

FIGURE 12 Frequency histogram of the mean *CWP* between 0600 and 1300 UTC of the different simulations and the observation. Date are averaged between 21°N–26.8°N and 53.8°E–59.5°E

Even if it is only a small member ensemble, simple probability maps for cloud-seeding applications can be derived. The probabilities were derived in the following way. Following Kniffka *et al.* (2014), a cloud is present in the model if $CWP \geq 0.05$ mm. If this is true for a model grid box, then this grid box is assigned a value of 1. This procedure is performed for each time step and each ensemble member. The resulting mask field is summed up and divided by the number of ensembles, so that a probability can be derived.

Figure 14 shows the model probability for cloud development at three different time steps (left column) and the corresponding CM–SAF *CWP* observations (right column). At 0700 UTC, none of the models simulates any clouds over the UAE, while the observation shows haze or low stratus clouds near the east coast of the UAE, which is a common feature during wet conditions (Aldababseh and Temimi, 2017). At 0900 UTC, the models show a high probability for clouds over the Al Hajar mountains, which is well in accordance with the observations. The model simulations even show a probability for clouds at the border between the UAE and Saudi Arabia, which appears to be a well known feature during summer (Figure 2 and Steinhoff *et al.*, 2018). During the mature stage of

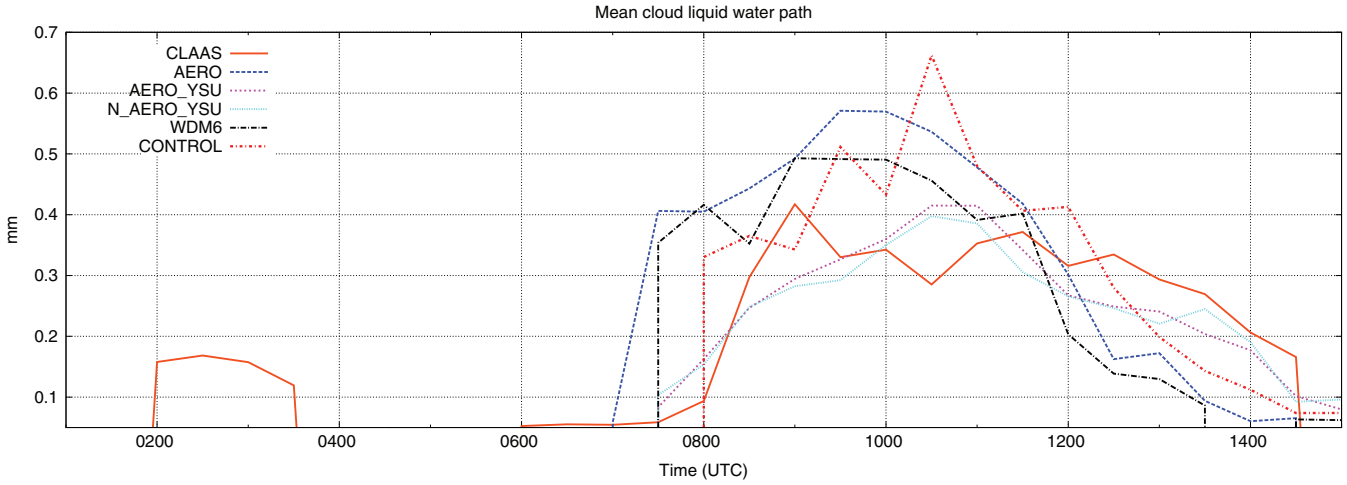

FIGURE 13 Area-averaged diurnal cycle of cloud liquid water path. The averaging area is 23.5°N–26°N and 55°E–57°E and mainly covers the Al Hajar mountains. Values of less than 0.05 mm are discarded

the convection around 1100 UTC, the model simulations show a high probability for clouds slightly west of the Al Hajar mountains, while the observations show clouds directly over the mountains. This shift could be due to the applied model resolution, which still might not be high enough to simulate the convergence at the correct location.

6.6 | Precipitation

Figure 15 shows the accumulated precipitation on 14 July, 2015. All WRF configurations do not simulate any precipitation and clouds beyond 1500 UTC, so that it is a valid approach to compare the simulations with the daily CHIRPS V2 data set.

The CHIRPS V2 data show moderate precipitation of up to 7 mm east of Al Ain, west of Hatta and near Dubai. The precipitation locations are in accordance with observations from the NCM precipitation radar network (not shown). While there is very little precipitation in the CONTROL simulation in these regions, the AERO simulation enhances the precipitation amount over the Al Hajar mountains with a similar maximum, but misses the precipitation event around Hatta and Dubai. As the only difference between both simulations is the application of water- and ice-friendly aerosols, they apparently help to enhance cloud and precipitation development. Interestingly, the AERO_YSU simulation shows less precipitation compared with the AERO simulation, although higher values of *CWP* are simulated. As shown in Figure 11, the lower (higher) amount of *CAPE* (*CIN*), compared with the AERO simulation, tends to inhibit more severe convection. The WDM6 experiment simulates a spot of about 15 mm on the Omani side of the Al Hajar mountains southeast of Al Ain, which is a lot more than observed, caused by an isolated single strong updraft. The N_AERO_YSU experiment is not shown, as there is almost no precipitation. This again points toward a benefit of applying at least an aerosol climatology combined with the Thompson cloud microphysics scheme.

7 | SUMMARY

This study investigated the potential of the WRF model to represent summertime convection over the UAE on July 14, 2015. The WRF model has been operated as a five-member physics ensemble at a convection-permitting resolution of 2.7 km with a dense vertical grid. The common set of physics parametrizations has been altered by applying the nonlocal YSU PBL scheme, the MYNN level 2.5 PBL scheme, the Thompson cloud microphysics scheme, the Thompson aerosol-aware cloud microphysics scheme, and the WDM6 2-moment cloud microphysics. The model results were validated against surface observations from NCM and MSG satellite products, as well as CHIRPS V2 gridded surface precipitation.

Over the desert regions of the UAE, the diurnal cycle of 2-m temperatures shows almost no systematic difference during daytime, while a negative bias is observed during the morning and evening transition. The differences present during the transition periods cannot be fully explained, but were also observed in a study of Fekih and Mohamed (2017) over the Algerian desert.

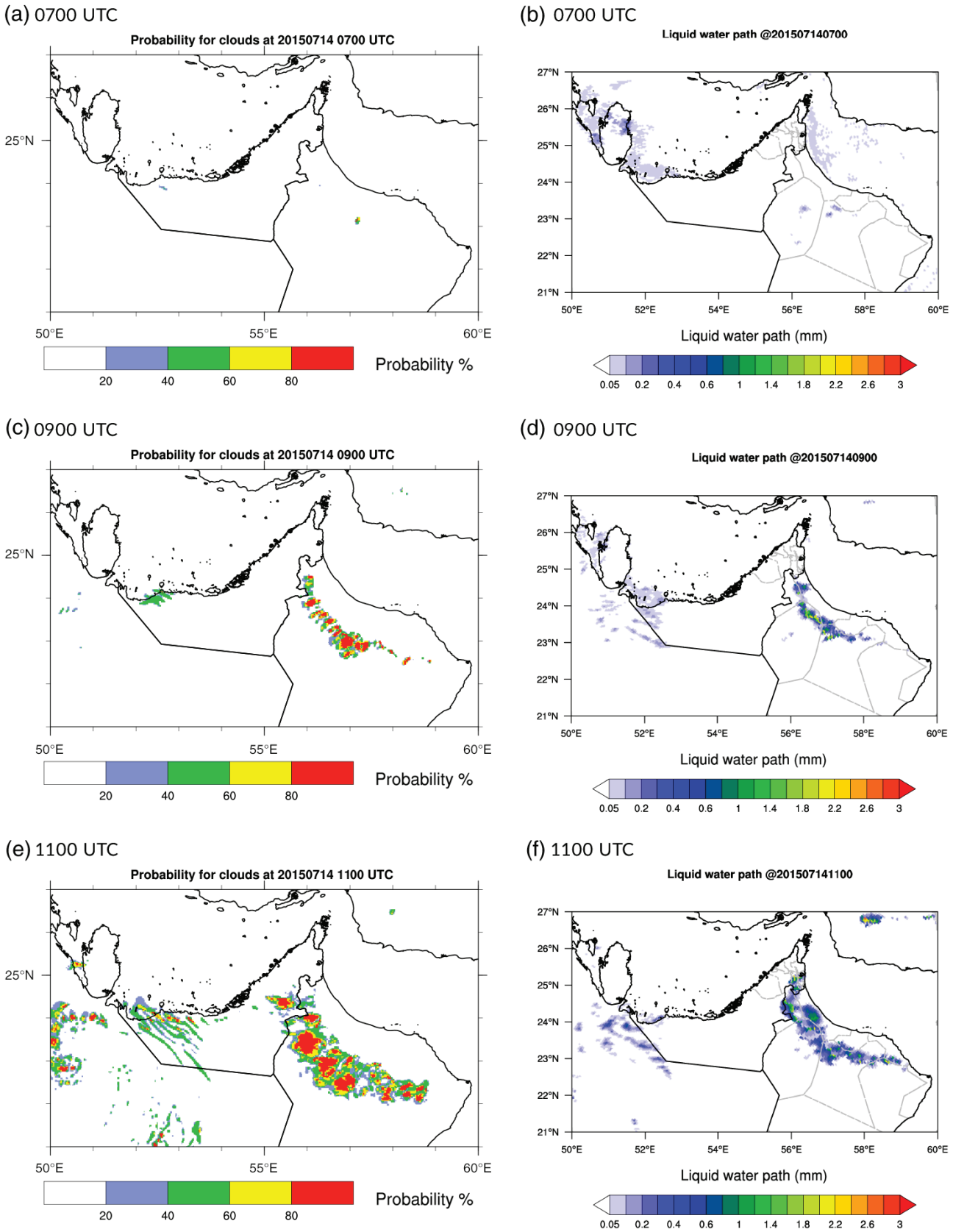

FIGURE 14 Cloud probability maps derived from the model ensemble at 0700, 0900, and 1100 UTC (left column) and the corresponding CM–SAF observations

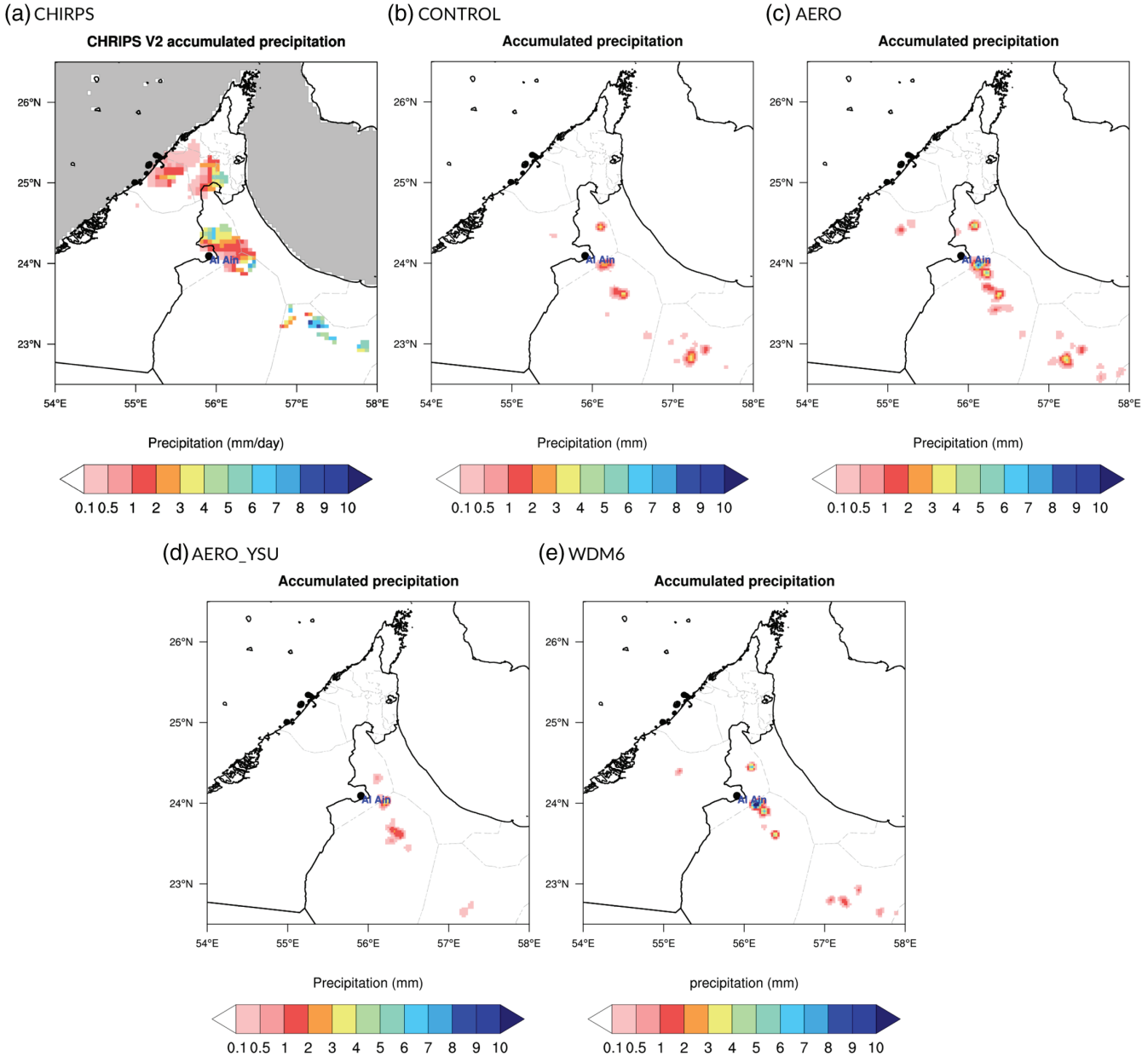

FIGURE 15 Accumulated precipitation on July 14, 2015, from (a) CHIRPS V2, (b) CONTROL simulation, (c) AERO, (d) AERO_YSU, and (e) WDM6 simulation

Interestingly, the mean 2-m dewpoint temperature over the western UAE follows the observations, showing correlations above 0.85. The RMSE is very similar in all simulations and shows only minor deviations during the whole day.

Considering the gradient Richardson number *Ri* (Figure 10), it appears that the MYNN PBL starts to spin up turbulence inside the PBL about 30 min earlier than the YSU PBL scheme. Also, the mixing appears to be stronger in the AERO simulation, as indicated by the higher wind velocities inside the PBL (Figure 9). Due to the lack of measurements, it is difficult to evaluate the individual performance of the different schemes. However, this can be overcome by the installation of a lidar network and flux measurements to complement each other in future (Wulfmeyer *et al.* 2018).

Simulations applying the MYNN PBL scheme predict stronger instabilities represented by higher (lower) values of *CAPE (CIN)* over the UAE, compared with simulations with the YSU PBL scheme.

A common challenge of all simulations is the simulation of clouds. Over the largest part of the model domain, the amount of CWP is underestimated, especially by the WDM6 simulation (Figure 12). The experiment with WDM6 microphysics simulates almost no liquid water clouds (Figure 12e), also reflected in the *SWDOWN* flux

fields (Figure 7e), with the best results obtained by the AERO simulation. Instead of liquid water clouds, the WDM6 simulation simulates a lot of thin ice clouds with integrated ice path (IWP) values of around 100 $g \cdot m^{-2}$ over the mountains, having very little effect on radiation. The main IWP contribution comes from altitudes between 4,700 and 5,500 m, which is the top of the PBL (Figure 9) and, according to the 1200 UTC radio sounding from Abu Dhabi, slightly above the level of free convection and the zero degree height.

Nevertheless, the diurnal cycle and the onset of convection over the Al Hajar mountains are well captured by all experiments. The application of a water- and ice-friendly aerosol climatology supports the cloud development, also with respect to more dense clouds. In the case in which the MYNN PBL scheme is replaced by the YSU PBL scheme, the model tends to produce more shallow clouds, which is also confirmed by the lower *SWDOWN* fluxes, especially as shown in the desert regions (Figure 7), associated with a negative SWDOWN bias of 30 $W \cdot m^{-2}$ compared with the AERO simulation.

From our results, it is valid to say that, for this particular case study, the application of water- and ice-friendly aerosols in combination with an aerosol-aware cloud microphysics and MYNN PBL is the most suitable combination to simulate convection over the UAE.

It is also shown that even a small physics ensemble is able to simulate the preconvective and convective environment reasonably. This will help to increase the reliability of potential cloud-seeding applications over the UAE. Future work will include a refinement of the ensemble design by adding more members, by not only changing the applied physics scheme but also varying parameters like surface roughness length, aerosol concentrations, or mixing length-scales. To enhance the process understating further, more summertime case studies and the application of variational data assimilation procedures have to be considered. This will help to further enhance process understanding and the understanding of the predictability of clouds and precipitation for cloud-seeding applications.

ACKNOWLEDGEMENTS

The authors thank the HLRS Stuttgart for providing the necessary computational resources within the WRFS-CALES project. ECMWF is acknowledged for providing the operational analysis data. The authors also thank the UAE National Center of Meteorology (NCM) for the quality-controlled weather station observations used in this study. This work was supported by the UAE Research Program for Rain Enhancement Science (UAEREP).

CONFLICT OF INTEREST

The authors declare no conflict of interest.

CODE AVAILABILITY STATEMENT

To download the WRF source code, users need to register on the following website: http://www2.mmm.ucar.edu/wrf/users/download/wrf-regist.php.

DATA AVAILABILITY STATEMENT

The data volume is about 9 TB for the simulations. Therefore, the data can be made available upon reqest with adequate prior notice. Using ECMWF analysis data requires a special agreement with ECMWF and DWD for data access and is usually limited to ECMWF member and cooperating states. Obtaining the weather station data from NCM in Abu Dhabi also requires an agreement.

ORCID

Thomas Schwitalla https://orcid.org/0000-0002-7898-8499

REFERENCES

Ackerman, S.A. and Cox, S.K. (1982) The Saudi Arabian heat low: aerosol distributions and thermodynamic structure. *Journal of Geophysical Research*, 87, 8991–9002. https://doi.org/10.1029/JC087iC11p08991

Al Mandoos, A. (2005). Synoptic and atmospheric stability classification for the United Arab Emirates. Master's dissertation, Johannesburg: University of Witwatersrand.

Albergel, C., de Rosnay, P., Gruhier, C., Munoz Sabater, J., Hasenauer, S., Isaksen, L., Kerr, Y. and Wagner, W. (2012) Evaluation of remotely sensed and modelled soil moisture products using global ground-based in situ observations. *Remote Sensing of Environment*, 118, 215–226

Aldababseh, A. and Temimi, M. (2017) Analysis of the long-term variability of poor visibility events in the UAE and the link with climate dynamics. *Atmosphere*, 8, 242

Argüeso, D., Hidalgo-Muñoz, J.M., Gámiz-Fortis, S.R., Esteban-Parra, M.J., Dudhia, J. and Castro-Díez, Y. (2011) Evaluation of WRF parametrizations for climate studies over Southern Spain using a multistep regionalization. *Journal of Climate*, 24, 5633–5651

Bae, S., Hong, S.-Y. and Lim, K.-S.S. (2016) Coupling WRF double-moment 6-class microphysics schemes to RRTMG radiation scheme in weather research forecasting model. *Advances in Meteorology*, 2016, 11.

Balsamo, G., Viterbo, P., Beljaars, A., van den Hurk, B., Hirschi, M., Betts, A. and Scipal, K. (2009) A revised hydrology for the ECMWF model: verification from field site to terrestrial water storage and impact in the integrated forecast system. *Journal of Hydrometeorology*, 10, 623–641

Bauer, H.-S., Schwitalla, T., Wulfmeyer, V., Bakhshaii, A., Ehret, U., Neuper, M. and Caumont, O. (2015) Quantitative precipitation estimation based on high-resolution numerical weather prediction and data assimilation with WRF – a performance test. *Tellus A*, 67, 25047

Bauer, H.-S., Weusthoff, T., Dorninger, M., Wulfmeyer, V., Schwitalla, T., Gorgas, T., Arpagaus, M. and Warrach-Sagi, K. (2011) Predictive skill of a subset of models participating in D-PHASE in the COPS region. *Quarterly Journal of the Royal Meteorological Society*, 137, 287–305. https://doi.org/10.1002/qj.715

Bennett, L.J., Blyth, A.M., Burton, R.R., Gadian, A.M., Weckwerth, T.M., Behrendt, A., Di Girolamo, P., Dorninger, M., Lock, S.-J., Smith, V.H. and Mobbs, S.D. (2011) Initiation of convection over the Black Forest Mountains during COPS IOP15a. *Quarterly Journal of the Royal Meteorological Society*, 137, 176–189. https://doi.org/10.1002/qj.760

Blanchard, D.O. (1998) Assessing the vertical distribution of convective available potential energy. *Weather and Forecasting*, 13, 870–877. https://doi.org/10.1175/1520-0434(1998)013<0870:ATVDOC>2.0.CO;2

Böer, B. (1997) An introduction to the climate of the United Arab Emirates. *Journal of Arid Environments*, 35, 3–16

Branch, O., Warrach-Sagi, K., Wulfmeyer, V. and Cohen, S. (2014) Simulation of semi-arid biomass plantations and irrigation using the WRF–NOAH model; a comparison with observations from Israel. *Hydrology and Earth System Sciences*, 18, 1761–1783

Branch, O. and Wulfmeyer, V. (2019) Deliberate enhancement of rainfall using desert plantations. *Proceedings of the National Academy of Sciences of the United States of America*, 116, 18841–18847

Breed, D., Bruintjes, R., Salazar, V. and Jensen, T. (2007). NCAR feasibility studies for weather modification programs over the past 10 years. Technical Report. Boulder, CO: Research Applications Laboratory (RAL), NationalCenter for Atmospheric Research (NCAR).

Bruintjes, R.T. (1999) A review of cloud seeding experiments to enhance precipitation and some new prospects. *Bulletin of the American Meteorological Society*, 80, 805–820

Chan, P.W. (2008) Determination of Richardson number profile from remote sensing data and its aviation application. *IOP Conference Series*, 1, 012043

Chaouch, N., Temimi, M., Weston, M. and Ghedira, H. (2017) Sensitivity of the meteorological model WRF–ARW to planetary boundary layer schemes during fog conditions in a coastal arid region. *Atmospheric Research*, 187, 106–127

Claußnitzer, A. and Névir, P. (2009) Analysis of quantitative precipitation forecasts using the dynamic state index. *Atmospheric Research*, 94, 694–703

Colarco, P., da Silva, A., Chin, M. and Diehl, T. (2010) Online simulations of global aerosol distributions in the NASA GEOS-4 model and comparisons to satellite and ground-based aerosol optical depth. *Journal of Geophysical Research*, 115, D14207. https://doi.org/10.1029/2009JD012820

Donlon, C.J., Martin, M., Stark, J., Roberts-Jones, J., Fiedler, E. and Wimmer, W. (2012) The operational sea surface temperature and sea ice analysis (OSTIA) system. *Remote Sensing of Environment*, 116, 140–158. Advanced Along Track Scanning Radiometer(AATSR) Special Issue

DTC (2017) *MET: Version 6.0 Model Evaluation Tools User's Guide*. NCAR, Boulder/CO. Available at: https://dtcenter.org/met/users/docs/users_guide/MET_Users_Guide_v6.1.pdf.

Eager, R.E., Raman, S., Wootten, A., Westphal, D.L., Reid, J.S. and Al Mandoos, A. (2008) A climatological study of the sea and land breezes in the Arabian Gulf region. *Journal of Geophysical Research*, 113, D15106

Ek, M.B., Mitchell, K.E., Lin, Y., Rogers, E., Grummann, P., Koren, V., Gayno, G. and Tarpley, J.D. (2003) Implementation of NOAH land surface model advances in the National Centers for environmental prediction operational mesoscale Eta model. *Journal of Geophysical Research*, 108, 8851

Evans, J.P., Ekström, M. and Ji, F. (2012) Evaluating the performance of a WRF physics ensemble over South-East Australia. *Climate Dynamics*, 39, 1241–1258. https://doi.org/10.1007/s00382-011-1244-5

Fekih, A. and Mohamed, A. (2017) Evaluation of the WRF model on simulating the vertical structure and diurnal cycle of the atmospheric boundary layer over Bordj Badji Mokhtar (southwestern Algeria). *Journal of King Saud University*, 31, 602–611

Findell, K.L. and Eltahir, E.A.B. (2003a) Atmospheric controls on soil moisture-boundary layer interactions: three-dimensional wind effects. *Journal of Geophysical Research*, 108, 8385. https://doi.org/10.1029/2001JD001515

Findell, K.L. and Eltahir, E.A.B. (2003b) Atmospheric controls on soil moisture? Boundary layer interactions. Part I: framework development. *Journal of Hydrometeorology*, 4, 552–569. https://doi.org/10.1175/1525-7541(2003)004<0552:ACOSML>2.0.CO;2

Finkensieper, S., Hanschmann, T., Stengel, M., Benas, N., van Zadelhoff, G.-J. and Meirink, J.-F. (2016a). Validation report SEVIRI cloud products CLAAS Edition 2. EUMETSAT. Technical Report. Available at: https://www.cmsaf.eu/SharedDocs/Literatur/document/2016/saf_cm_knmi_val_sev_cld_2_1_pdf.

Finkensieper, S., Meirink, J.-F., van Zadelhoff, G.-J., Hanschmann, T., Benas, N., Stengel, M., Fuchs, P., Hollmann, R. and Werscheck, M. (2016b) *CLAAS-2: CM SAF Cloud Property Dataset Using SEVIRI - Edition 2*. Satellite Application Facility on Climate Monitoring (CM SAF). Available at: https://doi.org/10.5676/EUM_SAF_CM/CLAAS/V002.

Funk, C., Peterson, P., Landsfeld, M., Pedreros, D., Verdin, J., Shukla, S., Husak, G., Rowland, J., Harrison, L., Hoell, A. and Michaelsen, J. (2015) The climate hazards infrared precipitation with stations a new environmental record for monitoring extremes. *Scientific Data*, 2. https://doi.org/10.1038/sdata.2015.66

Galligani, V.S., Wang, D., Alvarez Imaz, M., Salio, P. and Prigent, C. (2017) Analysis and evaluation of WRF microphysical schemes for deep moist convection over south-eastern South America (SESA) using microwave satellite observations and radiative transfer simulations. *Atmospheric Measurement Techniques*, 10, 3627–3649

García-Díez, M., Fernéndez, J., Fita, L. and Yagüe, C. (2013) Seasonal dependence of WRF model biases and sensitivity to PBL schemes over Europe. *Quarterly Journal of the Royal Meteorological Society*, 139, 501–514

Hammann, E., Behrendt, A., Le Mounier, F. and Wulfmeyer, V. (2015) Temperature profiling of the atmospheric boundary layer with rotational Raman lidar during the HD(CP)^2 observational prototype experiment. *Atmospheric Chemistry and Physics*, 15, 2867–2881

Heikenfeld, M., White, B., Labbouz, L. and Stier, P. (2019) Aerosol effects on deep convection: the propagation of aerosol perturbations through convective cloud microphysics. *Atmospheric Chemistry and Physics*, 19, 2601–2627

Hong, S.-Y. (2007). Stable boundary layer mixing in a vertical diffusion scheme. In: The Korea Meteor. Soc., Fall Conference, 25–26 October, Seoul, Korea.

Hong, S.-Y., Noh, Y. and Dudhia, J. (2006) A new vertical diffusion package with an explicit treatment of entrainment processes. *Monthly Weather Review*, 134, 2318–2341

Hong, S.-Y., Park, H., Cheong, H.-B., Kim, J.-E., Koo, M.-S., Jang, J., Ham, S., Hwang, S.-O., Park, B.-K., Chang, E.-C. and Li, H. (2013) The global/regional integrated model system (GRIMs). *Asia–Pacific Journal of Atmospheric Sciences*, 49, 219–243. https://doi.org/10.1007/s13143-013-0023-0

Iacono, M.J., Delamere, J.S., Mlawer, E.J., Shephard, M.W., Clough, S.A. and Collins, W.D. (2008) Radiative forcing by long-lived greenhouse gases: calculations with the AER radiative transfer models. *Journal of Geophysical Research*, 113, D13103

Inness, A., Baier, F., Benedetti, A., Bouarar, I., Chabrillat, S., Clark, H., Clerbaux, C., Coheur, P., Engelen, R.J., Errera, Q., Flemming, J., George, M., Granier, C., Hadji-Lazaro, J., Huijnen, V., Hurtmans, D., Jones, L., Kaiser, J.W., Kapsomenakis, J., Lefever, K., Leitão, J., Razinger, M., Richter, A., Schultz, M.G., Simmons, A.J., Suttie, M., Stein, O., Thépaut, J.-N., Thouret, V., Vrekoussis, M., Zerefos, C. and the MACC team (2013) The MACCreanalysis: an 8 yr data set of atmospheric composition. *Atmospheric Chemistry and Physics*, 13, 4073–4109

Jimenéz, P., Dudhia, J., Fidel González-Rouc, F., Navarro, J., Montávez, J. and Garcia-Bustamante, E. (2012) A revised scheme for the WRF surface layer formulation. *Monthly Weather Review*, 140, 898–918

Kendon, E.J., Ban, N., Roberts, N.M., Fowler, H.J., Roberts, M.J., Chan, S.C., Evans, J.P., Fosser, G. and Wilkinson, J.M. (2017) Do convection-permitting regional climate models improve projections of future precipitation change?. *Bulletin of the American Meteorological Society*, 98, 79–93

Khain, A.P., Leung, L.R., Lynn, B. and Ghan, S. (2009) Effects of aerosols on the dynamics and microphysics of squall lines simulated by spectral bin and bulk parametrization schemes. *Journal of Geophysical Research*, 114, D22203

Kniffka, A., Stengel, M., Lockhoff, M., Bennartz, R. and Hollmann, R. (2014) Characteristics of cloud liquid water path from SEVIRI onboard the Meteosat Second Generation 2 satellite for several cloud types. *Atmospheric Measurement Techniques*, 7, 887–905

Kottmeier, C., Kalthoff, N., Barthlott, C., Corsmeier, U., van Baelen, J., Behrendt, A., Behrendt, R., Blyth, A., Coulter, R., Crewell, S., di Girolamo, P., Dorninger, M., Flamant, C. and Foken, T. (2008) Mechanisms initiating deep convection over complex terrain during COPS. *Meteorologische Zeitschrift*, 17, 931–948. https://doi.org/10.1127/0941-2948/2008/0348

Lim, K.-S. and Hong, S.-Y. (2010) Development of an effective double-moment cloud microphysics scheme with progostic cloud condensation nuclei (CCN) for weather and climate models. *Monthly Weather Review*, 138, 1587–1612

Mahmoud, M.T., Hamouda, M.A. and Mohamed, M.M. (2019) Spatiotemporal evaluation of the GPM satellite precipitation products over the United Arab Emirates. *Atmospheric Research*, 219, 200–212

Mellor, G.L. and Yamada, T. (1974) A hierarchy of turbulence closure models for planetary boundary layers. *Journal of the Atmospheric Sciences*, 31, 1791–1806

Milovac, J., Ingwersen, J. and Warrach-Sagi, K. (2014) *Soil texture forcing data for the whole world for the Weather Research and Forecasting (WRF) model of the University of Hohenheim (UHOH) based on the Harmonized World Soil Database (HWSD) at 30 arc-second horizontal resolution*. World Data Center for Climate (WDCC). Available at: http://dx.doi.org/10.1594/WDCC/WRF_NOAH_HWSD_world_TOP_SOILTYP.

Milovac, J., Warrach-Sagi, K., Behrendt, A., Späth, F., Ingwersen, J. and Wulfmeyer, V. (2016) Investigation of PBL schemes combining the WRF model simulations with scanning water vapor dial measurements. *Journal of Geophysical Research*, 121, 624–649. https://doi.org/10.1002/2015JD023927

Mohalfi, S., Bedi, H.S., Krishnamurti, T.N. and Cocke, S.D. (1998) Impact of shortwave radiative effects of dust aerosols on the summer season heat low over Saudi Arabia. *Monthly Weather Review*, 126, 3153–3168. https://doi.org/10.1175/1520-0493(1998)126<3153:IOSREO>2.0.CO;2

Nakanishi, M. and Niino, H. (2006) An improved Mellor–Yamada level-3 model: its numerical stability and application to a regional prediction of advection fog. *Boundary-Layer Meteorology*, 119, 397–407

NASA (2011) *Tropical Rainfall Measuring Mission (TRMM) TMPA rainfall estimate l3 3 hour 0.25 degree x 0.25 degree v7*. Greenbelt, MD: Goddard Earth Sciences Data and Information Services Center (GES DISC). Available at: https://doi.org/10.5067/TRMM/TMPA/3H/7.

NCAR (2005). Rainfall enhancement assessment. Boulder, CO: National Center for Atmospheric Research. Assessment report. Available at: http://www.gccmet.net/libraries/download/5.

Nielsen, J. (2013). Representing vegetation processes in hydrometeorological simulations using the WRF model. PhD thesis, Roskilde, Denmark: DTU Wind Energy. No. 0016(EN) .

Niranjan Kumar, K. and Ouarda, T.B.M.J. (2014) Precipitation variability over UAE and global SST teleconnections. *Journal of Geophysical Research*, 119, 10313–10322

Niu, G., Yang, Z.-L., Mitchell, K., Chen, F., Ek, M., Barlage, M., Kumar, A., Manning, K., Niyogy, D., Rosero, E., Tewari, M. and Xia, Y. (2011) The community Noah land surface model with multiparametrization options (Noah-MP): 1. Model description and evaluation with local-scale measurements. *Journal of Geophysical Research*, 116, 19

Palmer, T. and Zanna, L. (2013) Singular vectors, predictability and ensemble forecasting for weather and climate. *Journal of Physics A*, 46, 254018. https://doi.org/10.1088%2F1751-8113%2F46%2F25%2F254018

Palmer, T.N. (2013) Climate extremes and the role of dynamics. *Proceedings of the National Academy of Sciences of the United States of America*, 110, 5281–5282

Patlakas, P., Stathopoulos, C., Flocas, H., Kalogeri, C. and Kallos, G. (2019) Regional climatic features of the Arabian Peninsula. *Atmosphere*, 10, 220

Prein, A.F., Langhans, W., Fosser, G., Ferrone, A., Ban, N., Goergen, K., Keller, M., Tölle, M., Gutjahr, O., Feser, F., Brisson, E., Kollet, S., Schmidli, J., van Lipzig, N.P.M. and Leung, R. (2015) A review on regional convection-permitting climate modeling: demonstrations, prospects, and challenges. *Reviews of Geophysics*, 53, 323–361. https://doi.org/10.1002/2014RG000475

Rácz, Z. and Smith, R.K. (1999) The dynamics of heat lows. *Quarterly Journal of the Royal Meteorological Society*, 125, 225–252. https://doi.org/10.1002/qj.49712555313

Ranjha, R., Tjernström, M., Semedo, A., Svensson, G. and Cardoso, R.M. (2015) Structure and variability of the Oman coastal

low-level jet. *Tellus A*, 67, 25285. https://doi.org/10.3402/tellusa.v67.25285

Schwitalla, T., Bauer, H.-S., Wulfmeyer, V. and Aoshima, F. (2011) High-resolution simulation over central Europe: assimilation experiments during COPS IOP 9c. *Quarterly Journal of the Royal Meteorological Society*, 137, 156–175

Schwitalla, T., Bauer, H.-S., Wulfmeyer, V. and Warrach-Sagi, K. (2017) Continuous high-resolution midlatitude-belt simulations for July–August 2013 with WRF. *Geoscientific Model Development*, 10, 2031–2055

Schwitalla, T., Bauer, H.-S., Wulfmeyer, V. and Zängl, G. (2008) Systematic errors of QPF in low-mountain regions as revealed by MM5 simulations. *Meteorologische Zeitschrift*, 17, 903–919

Sherif, M., Almulla, M., Shetty, A. and Chowdhury, R. (2014) Analysis of rainfall, PMP and drought in the United Arab Emirates. *International Journal of Climatology*, 34, 1318–1328. https://doi.org/10.1002/joc.3768

Shin, H.H. and Hong, S.-Y. (2011) Intercomparison of planetary boundary-layer parametrizations in the WRF model for a single day from cases-99. *Boundary-Layer Meteorology*, 139, 261–281

Skamarock, W.C., Klemp, J.B., Dudhia, J., Gill, D., Barker, D.O., Duda, M.G., Wang, W. and Powers, J.G. (2008). A description of the advanced research WRF version 3. Boulder, CO: NCAR. NCAR Technical Note TN-475+STR. Available at: http://www.mmm.ucar.edu/wrf/users/docs/arw_v3.pdf.

Song, H.-J. and Sohn, B.-J. (2018) An evaluation of WRF microphysics schemes for simulating the warm-type heavy rain over the Korean peninsula. *Asia–Pacific Journal of Atmospheric Sciences*, 54, 225–236. https://doi.org/10.1007/s13143-018-0006-2

Späth, F., Behrendt, A., Muppa, S.K., Metzendorf, S., Riede, A. and Wulfmeyer, V. (2016) 3-d water vapor field in the atmospheric boundary layer observed with scanning differential absorption lidar. *Atmospheric Measurement Techniques*, 9, 1701–1720

Steeneveld, G.J., Ronda, R.J. and Holtslag, A.A.M. (2015) The challenge of forecasting the onset and development of radiation fog using mesoscale atmospheric models. *Boundary-Layer Meteorology*, 154, 265–289

Steinhoff, D.F., Bruintjes, R., Hacker, J., Keller, T., Williams, C., Jensen, T., Al Mandous, A. and Al Yazeedi, O.A. (2018) Influences of the monsoon trough and Arabian heat low on summer rainfall over the United Arab Emirates. *Monthly Weather Review*, 146, 1383–1403. https://doi.org/10.1175/MWR-D-17-0296.1

Stephens, G.L. (1978) Radiation profiles in extended water clouds. II: parametrization schemes. *Journal of the Atmospheric Sciences*, 35, 2123–2132

Strobach, E. and Bel, G. (2019) Regional decadal climate predictions using an ensemble of WRF parametrizations driven by the MIROC5 GCM. *Journal of Applied Meteorology and Climatology*, 58, 527–549. https://doi.org/10.1175/JAMC-D-18-0051.1

Tegen, I., Hollrig, P., Chin, M., Fung, I., Jacob, D. and Penner, J. (1997) Contribution of different aerosol species to the global aerosol extinction optical thickness: estimates from model results. *Journal of Geophysical Research*, 102, 23895–23915. https://doi.org/10.1029/97JD01864

Thompson, G. and Eidhammer, T. (2014) A study of aerosol impacts on clouds and precipitation development in a large winter cyclone. *Journal of the Atmospheric Sciences*, 71, 3636–3658. https://doi.org/10.1175/JAS-D-13-0305.1

Thompson, G., Field, P.R., Rasmussen, R.M. and Hall, W.D. (2008) Explicit forecasts of winter precipitation using an improved bulk microphysics scheme. Part II: implementation of a new snow parametrization. *Monthly Weather Review*, 136, 5095–5115

Thompson, G., Tewari, M., Ikeda, K., Tessendorf, S., Weeks, C., Otkin, J. and Kong, F. (2016) Explicitly-coupled cloud physics and radiation parametrizations and subsequent evaluation in WRF high-resolution convective forecasts. *Atmospheric Research*, 168, 92–104

Trigo, I.F., Dacamara, C.C., Viterbo, P., Roujean, J.-L., Olesen, F., Barroso, C., de Coca, F.C., Carrer, D., Freitas, S.C., García-Haro, J., Geiger, B., Gellens-Meulenberghs, F., Ghilain, N., Meliá, J., Pessanha, L., Siljamo, N. and Arboleda, A. (2011) The satellite application facility for land surface analysis. *International Journal of Remote Sensing*, 32, 2725–2744

Warner, T.T. (2004) *Desert Meteorology*. Cambridge, UK: Cambridge University Press.

Weckwerth, T.M., Horst, T.W. and Wilson, J.W. (1999) An observational study of the evolution of horizontal convective rolls. *Monthly Weather Review*, 127, 2160–2179

Weckwerth, T.M., Wilson, J.W., Wakimoto, R.M. and Crook, N.A. (1997) Horizontal convective rolls: determining the environmental conditions supporting their existence and characteristics. *Monthly Weather Review*, 125, 505–526

Wehbe, Y., Ghebreyesus, D., Temimi, M., Milewski, A. and Mandous, A.A. (2017) Assessment of the consistency among global precipitation products over the United Arab Emirates. *Journal of Hydrology*, 12, 122–135

Wehbe, Y., Temimi, M., Weston, M., Chaouch, N., Branch, O., Schwitalla, T., Wulfmeyer, V., Zhan, X., Liu, J. and Al Mandous, A. (2019) Analysis of an extreme weather event in a hyper-arid region using WRF-hydro coupling, station, and satellite data. *Natural Hazards and Earth System Sciences*, 19, 1129–1149

Weijenborg, C., Friederichs, P. and Hense, A. (2015) Organisation of potential vorticity on the mesoscale during deep moist convection. *Tellus A*, 67, 25705. https://doi.org/10.3402/tellusa.v67.25705

Wulfmeyer, V., Behrendt, A., Kottmeier, C., Corsmeier, U., Barthlott, C., Craig, G.C., Hagen, M., Althausen, D., Aoshima, F., Arpagaus, M., Bauer, H.-S., Bennett, L., Blyth, A., Brandau, C., Champollion, C., Crewell, S., Dick, G., DiGirolamo, P., Dorninger, M., Dufournet, Y., Eigenmann, R., Engelmann, R., Flamant, C., Foken, T., Gorgas, T., Grzeschik, M., Handwerker, J., Hauck, C., Höller, H., Junkermann, W., Kalthoff, N., Kiemle, C., Klink, S., König, M., Krauss, L., Long, C.N., Madonna, F., Mobbs, S., Neininger, B., Pal, S., Peters, G., Pigeon, G., Richard, E., Rotach, M.W., Russchenberg, H., Schwitalla, T., Smith, V., Steinacker, R., Trentmann, J., Turner, D.D., van Baelen, J., Vogt, S., Volker, H., Weckwerth, T., Wernli, H., Wieser, A. and Wirth, M. (2011) The Convective and Orographically Induced Precipitation Study (COPS): the scientific strategy, the field phase, and research highlights. *Quarterly Journal of the Royal Meteorological Society*, 137, 3–30

Wulfmeyer, V., Turner, D.D., Baker, B., Banta, R., Behrendt, A., Bonin, T., Brewer, W.A., Buban, M., Choukulkar, A., Dumas, E., Hardesty, R.M., Heus, T., Ingwersen, J., Lange, D., Lee, T.R., Metzendorf, S., Muppa, S.K., Meyers, T., Newsom, R., Osman, M., Raasch, S., Santanello, J., Senff, C., Späth, F., Wagner, T.

and Weckwerth, T. (2018) A new research approach for observing and characterizing land–atmosphere feedback. *Bulletin of the American Meteorological Society*, 99, 1639–1667. https://doi.org/10.1175/BAMS-D-17-0009.1

Zhu, K. and Xue, M. (2016) Evaluation of WRF-based convection-permitting multi-physics ensemble forecasts over china for an extreme rainfall event on 21 July 2012 in Beijing. *Advances in Atmospheric Sciences*, 33, 1240–1258. https://doi.org/10.1007/s00376-016-6202-z

How to cite this article: Schwitalla T, Branch O, Wulfmeyer V. Sensitivity study of the planetary boundary layer and microphysical schemes to the initialization of convection over the Arabian Peninsula. *QJR Meteorol Soc*. 2020;146:846–869. https://doi.org/10.1002/qj.3711